Modelling seafloor methane discharge at the Landsort deep seep site

Grim Zetterlund

Abstract

In 2023, a 17 km^2 ebullition field was discovered near the deepest part of the Baltic sea, at the Landsorts deep. The seep site is located in the largest marine dead zone in the world, with an area of 70 000 km^2. The combination of eutrophication, baltic sea circulation patterns and a high accumulation rate of organic material have led to high rates of methane gas flux from the seafloor, estimated to at least 1 mol/m^2/year through acoustic data. Methane is a potent greenhouse gas with significant impact on the atmosphere on both short and long time scales, and understanding the underlying behaviours of methane seepage systems is important for global climate studies. Previous research on methanogenesis in the area have focused on in situ measurements of methane content along with acoustic surveys. This study investigates whether the geomechanical flow simulator TOUGH+HYDRATE can reproduce the observed methane seepage at the Landsort deep, something that has never been done before. The model incorporates methanogenesis, gas migration, fracture dynamics, anaerobic oxidation of methane (AOM) and phase changes. We also set out to find the underlying mechanisms and parameters that control the methane flux in the area. This research suggests that TOUGH+HYDRATE can reproduce the methane fluxes comparable to the ones observed at the Landsort deep. Among the tested parameters, the depth and rate of methane production exerted the most control on methane gas flux from the seafloor. The results also show that seeping systems like the landsort deep are sensitive to variations in sediment physical properties such as porosity, grain density, cohesion and tensile strength, coupled with the depth and rate of methanogenesis. These were shown to create a sensitive relationship between the free gas depth and different methane flux behaviours, that varies greatly when tuning these parameters. This relationship suggests that observations of the free gas depth may be used to infer physical properties of sediments and improve the characterization of methane seep systems.

Keywords: Methane seepage, Fracture-mediated flow, Marine sediments, TOUGH+HYDRATE, Landsort Deep, Baltic Sea, Methanogenesis, Geomechanical modelling, Free gas migration, Permanently fractured zone (PFZ)

TABLE OF CONTENTS

List of Figures and Tables

List Of Figures

List Of Tables

Abbreviations

AOM	Anaerobic Oxidation of Methane
CH_4	Methane
CO_2	Carbon Dioxide
KYR	Thousand Years
MBSF	Meters Below Sea Floor
MCD	Meters Composite Depth
PFZ	Permanently Fractured Zone
SMTZ	Sulfate-Methane Transition Zone
SO_4^{2-}	Sulfate
SRZ	Sulfate Reduction Zone
Tg	Teragram (10^{12} grams)
VPD	Vertical CH_4 Production Distribution Width

1. Introduction

Methane (CH_4) is a greenhouse gas up to 30 times more potent than CO_2 over a 100 year timescale and up to 84 times more potent over a 20 year period (Egger et al., 2017; Ruppel & Kessler, 2017; Liu et al., 2022). The contribution of methane from marine sediments to the atmospheric CH_4 budget is not well constrained in the literature, but the global flux has been estimated between 6-12 Tg CH_4 Yr^{-1} (Judd, 2004; Howarth et al., 2011; Howarth, 2014; Egger et al., 2017; Weber et al., 2019; Liu et al., 2022). Due to oxidation of methane in the water column, the amount that escapes the seafloor and goes into the water column has been estimated to be between 16 to 3200 Tg/year, which reflects that measuring this flux is difficult and often varies very much spatially (Liu et al., 2017; Ruppel & Kessler, 2017). Methane from marine sediment generally comes from either biogenic degradation of organic matter in anoxic conditions (Lenstra et al., 2023) or through the same processes that create petroleum oil in deep sediments (thermogenic production, Judd, 2004). In both pathways, if specific conditions are satisfied, the CH_4 can also form crystalline-like structured compounds known as gas hydrates, which start to dissociate when as a response to e.g seafloor warming or falling sea levels and subsequent mobilization of free CH4 gas . The CH_4 can also be formed and released from sediments without gas hydrates forming (Koh et al., 2002; Judd, 2004). The methane seepage in the Landsort deep is caused by biogenic processes and, due to fairly shallow seafloors (< 460 m), also does not form hydrates (Egger et al., 2017; Ketzer et al., 2024).

The global rate of CH_4 production in marine sediments has been estimated to be between 85-300 Tg / year, however approximately 90% of that gets consumed by microorganisms such as sulfate reducing bacteria as well iron oxide reducing bacteria in a process known as anaerobic oxidation of methane (AOM) before reaching the seafloor. If iron oxide is coupled, such as it is suggested to be in the Landsort deep, either directly where the iron oxide acts as the electron acceptor or indirectly where iron oxides stimulates the reduction of SO_4^{2-} , it is generally referred to as Fe-AOM (Knittel & Boetius, 2009; Riedinger et al., 2014; Egger et al., 2017).

The landsort deep is the deepest part of the baltic sea, reaching at its maximum depth 459 m, and due to bottom currents a lot of organic material has accumulated there during the last 100 years (Winterhalter et al., 1981; Ketzer et al., 2024). The recently discovered ebullition site is located in the largest human induced dead zone in the world, with an area of 70 000 km^2, surpassing the second largest in the gulf of Mexico threefold (Ketzer et al., 2024). It has been estimated to release methane in fluxes of around 1 mol / m^2 / year, based on hydroacoustic surveys (Christian Stranne, personal communication, 2026), and covers an area of 17 km^2 (Felip et al., 2025). Figure 1 shows the ebullition field, along with a marked EK80 transect for acoustic interpretation and an overview map for reference. The current hypothesis is that the ebullition field is associated with a drift deposit, where the high sediment accumulation rate (>1 cm / year) leads to high rates of methanogenesis in the sediments, and also inhibits the sulfate reducing bacteria somewhat in filtering the CH_4 (Ketzer et al., 2024). The AOM filter is able to take care of most of the dissolved advection of CH_4 but has been shown to be inhibited when gas is released through fractures in low permeable sediments ($>10^{-15.75} m^2$), which was demonstrated by modelling in Stranne et al., (2022) to make the AOM filter almost obsolete under certain time scales and emission scenarios. This, also coupled with the fact that the sulfate concentrations in these bottom waters is generally low due to low seawater salinities in the Baltic Sea, ultimately leads to an almost unregulated methane flux (Ketzer et al., 2024).

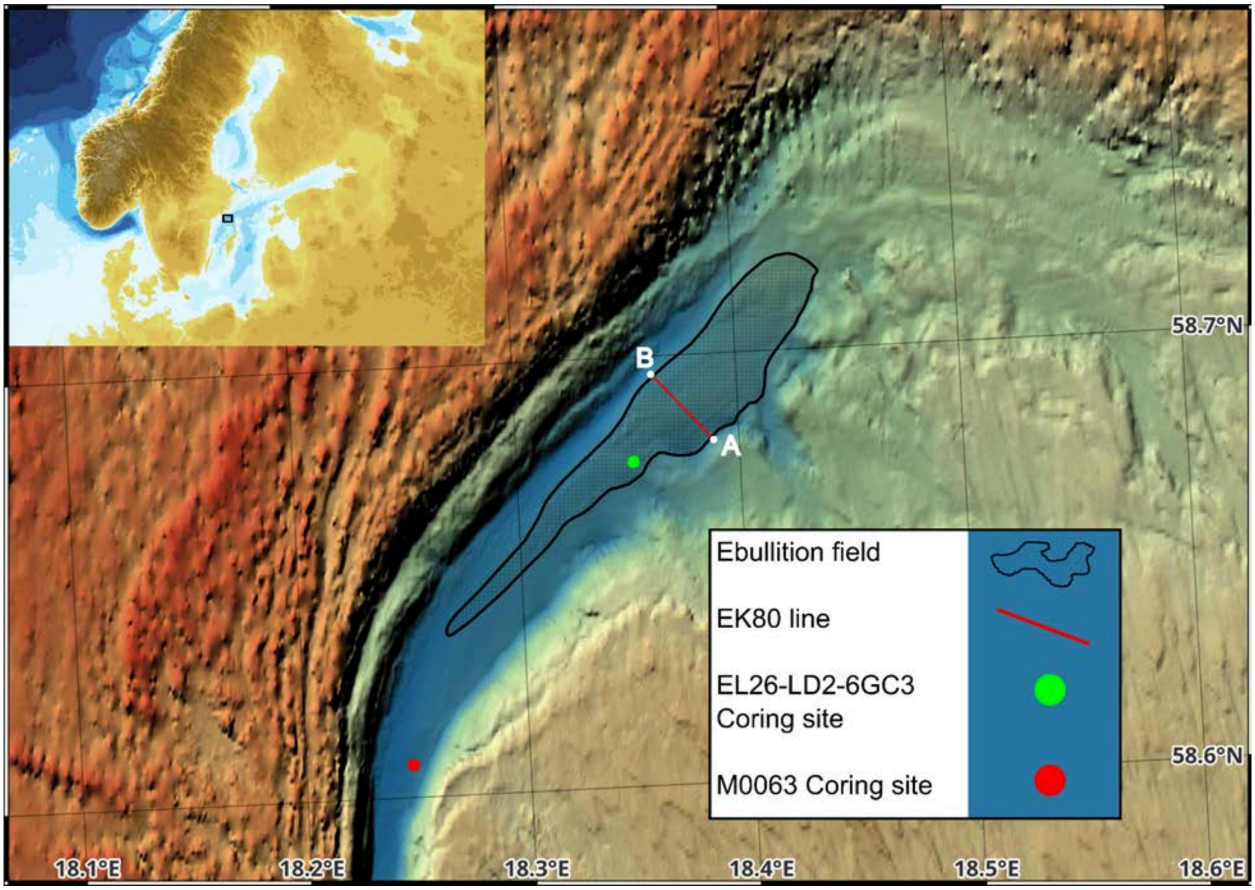

Figure 1. Overview map of the Landsort deep seep site, with coring site for EL26-LD2-GC6 and IODP expedition 347 hole M0063 (Expedition 347 Scientists, 2014) marked, ebullition field and EK80 line used in Figure 2 (red line, B - A). Bathymetry data from EMODnet bathymetry consortium (2024).

The interplay of methanogenesis, AOM and sediment gas flow dynamics is not well understood (Knittel & Boetius, 2009) and a modelling of the seepage in the Landsort deep has never been conducted before. Other studies in the area have primarily looked at dissolved CH_4 in porewater samples as well as modelling CH_4 production based on said porewater samples, along with some acoustic and seismic surveying (Flury et al., 2016; Egger et al., 2017; Ketzer et al., 2024) but never has geomechanical and AOM coupling been modeled against observations. Here, we use the multi-phase methane transport model TOUGH+HYDRATE and tune the model parameters in such fashion that the output matches the observed seepage. The aim is to tune multiple parameters in order to isolate the dominant controls on different behaviours of the simulated methane system as well as to investigate the feasibility of our results by comparing them to real world observations. The research goals can essentially be formulated as:

- (1) Understand the mechanisms and parameters that control the methane flux in the area
- (2) Investigate the possibility of using the TOUGH+HYDRATE model in future research of the same and similar seep sites.

2. Background

2.1 Methane in marine sediments

Methane is produced in marine sediments by methanogenic archaea in hypoxic or anoxic conditions, where they consume organic material anaerobically. Methane flux from marine sediments is mitigated by the AOM in the SRZ. The base of the SRZ is usually referred to as the SMTZ, defined as the interface where the concentration of sulfate and methane is equal (Lenstra et al., 2023; Lapham et al., 2024). When the sulfate concentration decreases, the net production of methane increases, and peaks somewhere underneath the SMTZ (Reeburgh, 2007; Flury et al., 2016; Dale et al., 2019). The depth of the SMTZ is dependent on sedimentation rate, depth of methane production, as well as methane and sulfate fluxes and consumption rates (Knittel & Boetius, 2009; Egger et al., 2017; Barker Jørgensen et al., 2024).

2.2 Methane transport mechanisms

Dissolved methane moves upward due to a gradient in concentration, in a process called diffusion. It has been found that diffusion of methane in marine sediments is not an efficient path for methane migration as it can take months to pass a ten centimeter sediment column, and it is estimated that around 1% of global diffusive methane flow reaches the seafloor due to AOM (Liu et al., 2022). Advection is the transport by the bulk motion of fluids and can be both through dissolved and free gas flow, free gas flow through sediment matrix or through hydraulic fractures created by overpressure in pore space. If the water gets oversaturated with methane, bubbles will form and eventually move upward through the sediment column by its buoyant force and then escape the seafloor. In low permeability sediments, as observed at the study site, the gas will subsequently escape from the seafloor as a gas plume through a fracture initiated by overpressure exerted by the gas phase in pore space (Behrmann et al., 2006; Boudreau, 2012; Stranne et al., 2017). When methane moves as a free gas in the sediments, the AOM has little to no effect on it since AOM can only utilize dissolved methane (Liu et al., 2022; Stranne et al., 2022; Lapham et al., 2024).

2.3 Landsort deep seep site

Large parts of the Baltic sea are heavily eutrophied and the water column is also very stratified, thus bottom waters can be severely hypoxic and even anoxic (Rönnberg & Bonsdorff, 2004), such is the case at the Landsort deep. Due to bottom currents, the sedimentation rate at the site is also very high, surpassing 1 cm / year with most of it being organic material. This leads to high anaerobic productivity in the sediments producing CH4, an ineffective AOM filter and an easier buildup of pore overpressure (Behrmann et al., 2006; Ketzer et al., 2024; Lapham et al., 2024). There is a risk that with increasing temperatures eutrophication will also increase, potentially leading to even more methane produced in a positive feedback loop (Ketzer et al., 2024). It has also been suggested that methane is migrating downward into older sediments deposited after the last glaciation (9-7 Kyr), making those deposits a sink for methane (Egger et al., 2017). This suggests an abundance of methane stored in the deeper parts of the sediments. Acoustic data from the seeping site shows gas bubbles migrating through the water columns, as well as the free gas depth.

The free gas depth changes somewhat over the measured area, something interpreted from acoustic data in Figure 2, which is something that we tuned the model to match. It can be interpreted as the depth of the base of the permanently fractured zone (PFZ), a certain depth that occurs in TOUGH+HYDRATE simulations where the capillary pressure exerted on the sediment by the gas is high enough for the sediments to form semi permeable fractures, leading to a fast release of gas once it is reached (Stranne et al., 2017). The PFZ is explained in more detail further onward.

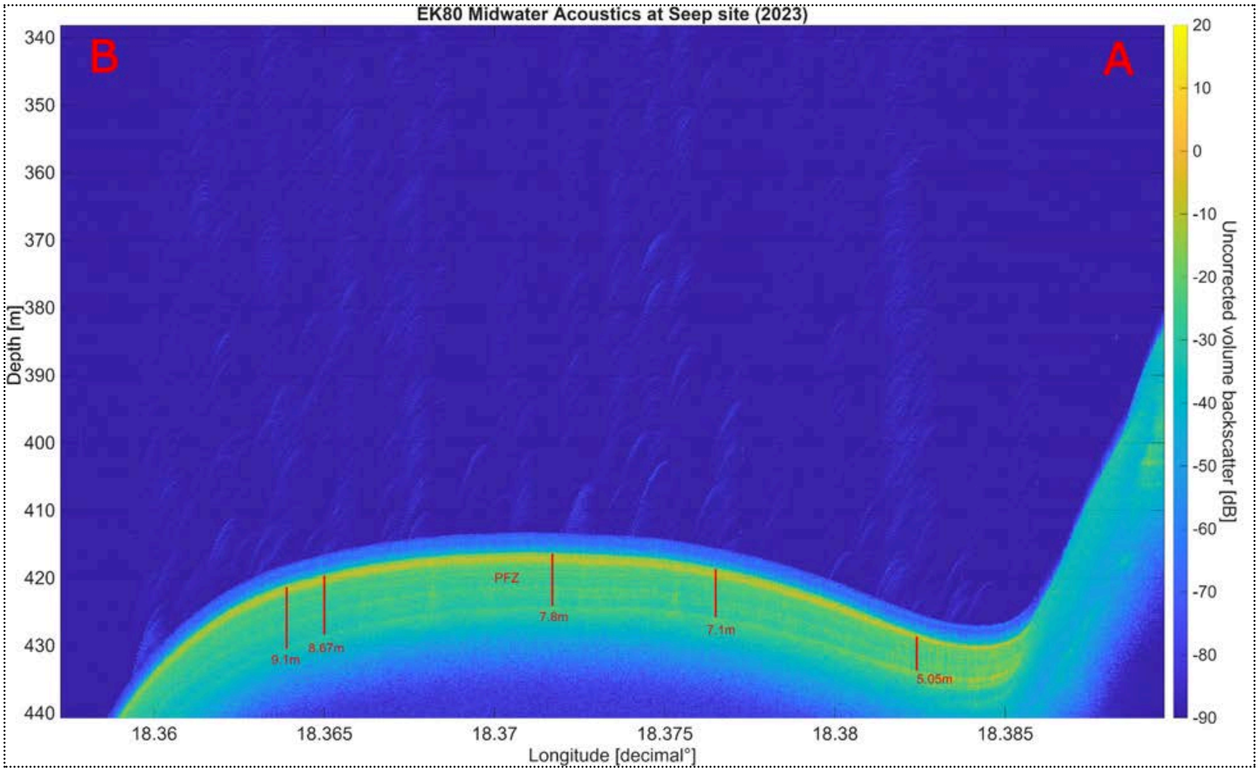

Figure 2. Simrad EK80 midwater acoustic data from the active seep site. The permanently fractured zone (PFZ) has been visually interpreted (red lines) at five different coordinates. The EK80 line is marked in Figure 1 with approximated locations of labels B and A.

2.4 Modeling methane systems

Methane transport involves a number of coupled processes that together can be complex to parameterize, such as diffusion, advection, free gas migration, phase changes, fracture formation and AOM (Liu et al., 2022). There is also a lot of spatial and temporal variability in real world seepage systems, and it is important to note that this modelling is made in 1 dimension, which can be hard to visualize and conceptually grasp, especially when analysing fracture formation and gas propagation. It essentially collapses the entire seepage area to a 1D column where the flux is measured in mol/m^2/year.

Other studies have modeled and measured CH_4 production in the area and baltic proper, but they have been based on porewater samples and have not included geomechanical fracture flow nor been compared to real life observations of methane seepages (Flury et al., 2016; Egger et al., 2017; Dale et al., 2019; Ketzer et al., 2024). Fracture flow has been shown to be one of the most important transportation methods of methane in low permeability sediments (Boudreau, 2012; Stranne et al., 2017) which these other studies have not accounted for. TOUGH+HYDRATE solves heat and mass balance equations to model the flow of gas and fluids in complex geological media as long as Darcy's law is valid (Moridis, 2014). This study focuses on fracture flow, methanogenesis location in relation to the free gas depth and seepage periodicity.

3. Method

3.1 Model setup

In short, the parameters that were tuned and tested were as follows:

- The CH_4 production source (**Q**) which describes the simulated production rate of methane in the sediments.
- The Vertical CH_4 production distribution width (**VPD**), describing the start and end depths of a gaussian function, over which the earlier mentioned **Q** is integrated over.
- The fracture threshold (***λ****), essentially a parameter that describes how easily hydraulic fractures form in the sediments.
- Fracture permeability ($\boldsymbol{k_f}$), describing the permeability of hydraulic fractures, mainly affecting the migration speed of gas.
- Other physical properties such as grain density (***ρ***) and porosity (***Φ***) along with seafloor depth (**Z**) were also tested.

Further details about each parameter are described in their own parts of the method section.

To investigate which parts of the system that different parameters affect, a total of 55 cases with varying parameter values were run. A base case was chosen to recreate the observed seepage, where the vertical CH_4 distribution production width was based on the shallow peak of modeled methanogenesis in Egger et al., (2017) at ~6.25m, the CH_4 production source was based on observed seepage, while the other parameters were chosen based on the physical properties at the site. The average fluxes of the simulation runs were calculated for a 100 year window or once the system reached steady-state.

Every parameter tested is listed in Table 1. When describing simulation cases, they are mentioned as their parameters symbol followed by the value in subscript. E.g. the simulation case where porosity is set to 0.7 is named "$\boldsymbol{\Phi}_{0.7}$". When mentioning multiple cases, the values for said cases are also in subscript, inside of brackets, separated by a semicolon: $\boldsymbol{\Phi}_{[0.6\ ;\ 0.8]}$. If an entire range of values are mentioned, the maximum and minimum are separated in subscript by a dash: $\boldsymbol{\Phi}_{[0.6-0.8]}$. If describing cases where parameter values greater or lesser than, for example, $\boldsymbol{\Phi} > 0.8$, the notation used is $\boldsymbol{\Phi}_{[>0.8]}$.

Table 1. Every parameter tested in the model.

Parameter	Symbol	Number of tests (+ base case)	Testing range	Base case
CH_4 production source	$\boldsymbol{Q}$	7	10^{-9} - 8×10^{-9} kg/m²/s	10^{-9} kg/m²/s
Vertical CH_4 production distribution width	***VPD***	7	0.1-10 m - 0.1-40 m	0.1-12.5 m
Fracture permeability	$\boldsymbol{k_f}$	8	10^{-11} - 10^{-9} m²	10^{-10} m²
Fracture threshold	$\boldsymbol{\lambda^*}$	9	0.8 - 1.35	1.2
Vertical resolution	***R***	6	1.97 - 9.4 cm	2.64 cm
Porosity	$\boldsymbol{\Phi}$	12	0.6 - 0.95	0.82
Water depth	***Z***	3	51 - 418.2 m	418.2 m
Grain density	$\boldsymbol{\varrho}$	10	2400 - 2900 kg/m³	2572 kg/m³

When simulating using the standard vertical resolution ($\mathbf{R}_{2.64\ cm}$), the model is set up with 960 grid cells, 946 of which are evenly spaced for the first 25 m (~2.64 cm / cell) and 14 grid cells from 25 to 400mbsf, with their sizes increasing logarithmically downwards. For the cases with wider vertical CH_4 production distribution widths ($\mathbf{VPD}_{[0.1\text{-}30;\ 0.1\text{-}40m]}$) the shallow part is extended to 40m out of necessity, which results in a drop in final resolution. For 5 cases we analyze a range of different grid-cell resolutions to see if they have any substantial impact on the fractures and the flux frequencies: $\mathbf{R}_{[9.4;\ 4.45;\ 2.35;\ 2.1;\ 1.97\ cm]}$. The goal was to reach a maximum resolution that afterward especially the permeability and flux frequencies will not be impacted after further increase of said resolution, referred to as convergence.

3.2 Physical properties

Sediment physical properties were sampled from sediment cores from the area. Permeability, grain density and porosity were gathered from the gravity core EL26-LD2-6GC3. Heat flow, dry and wet conductivity were calculated using data from IODP expedition 347 hole M0063 [A-E] datasets (Expedition 347 Scientists, 2014). The heat flow was calculated by first using thermal conductivity and temperature data to calculate the thermal resistivity. The thermal conductivity was plotted against depth (MCD) and its linear regression was used to extrapolate a continuous thermal conductivity curve that was then used, along with the measured conductivities, to calculate thermal resistivity. After this, the thermal resistivity was plotted against temperature, known as a Bullard plot (Figure 3), following Bullard, (1939). The Bullard plot gives the heat flow as 19.2 mW/m². The grain density was estimated to 2572 kg/m³, permeability to 10^{-16}m², and fractional porosity to 0.82. Both dry and wet thermal conductivities were calculated to 0.0489 and 0.573 $Wm^{-1}K^{-1}$ respectively (Table 2).

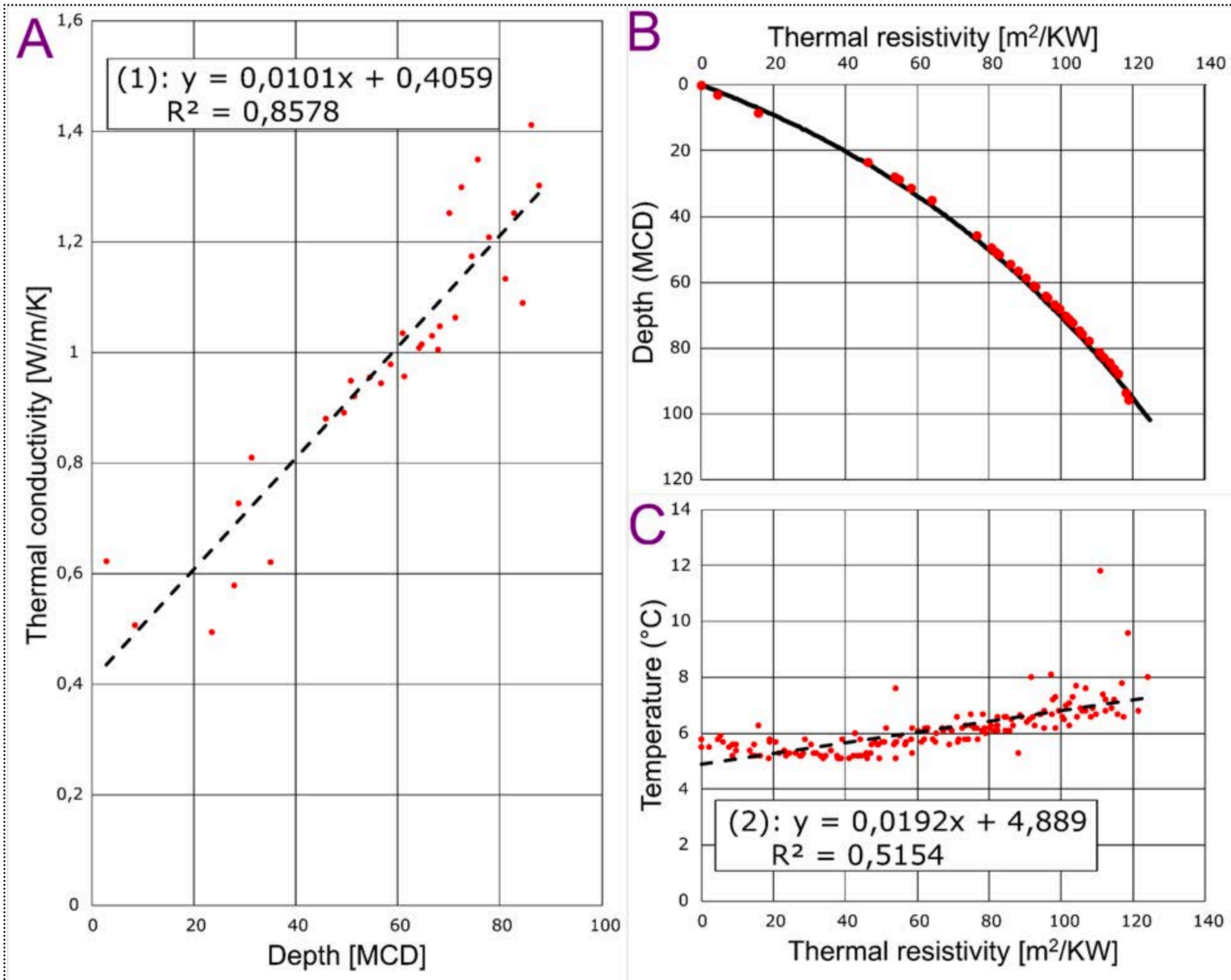

Figure 3. A: Depth (mcd) vs Thermal conductivity from IODP expedition 347, hole M0063 [A-E] (Expedition 347 Scientists, 2014). B: Thermal resistivity calculated from observed thermal conductivities (red points), as well as from an extrapolated continuous thermal conductivity curve using the linear regression equation (1) from 2A (black line). C: Bullard plot: Measured temperature vs thermal resistivity to estimate heat flow (Bullard, (1939)). The linear regression (0.0192, equation (2)) is the heat flow, and the intersection (~4.9) is the temperature at the seafloor in °C.

Table 2. physical properties. The grain density and porosity were also tested as parameters, as shown in Table 1.

Porosity (fractional)	**Grain density** (kgm^{-3})	**Permeability** (m^2)	**Heat flow** (mWm^{-2})	**Wet conductivity** ($Wm^{-1}K^{-1}$)	**Dry conductivity** ($Wm^{-1}K^{-1}$)
Φ	ϱ	k	q	λ_w	λ_d
0.82	2572	10^{-16}	19.2	0.56	0.04

3.3 Methane production module

The methane production in marine sediments is directly linked to the AOM, due to the relationship between the methanogenic and methanotrophic microbes and thus indirectly to the content of sulfate.

Because of this, the methane production in marine sediments as a function of depth commonly takes a concave shape, increasing as sulfate content decreases (Reeburgh, 2007; Knittel & Boetius, 2009; Flury et al., 2016; Dale et al., 2019). To simulate this, we introduce a simplified approximation of methanogenesis beneath the SRZ in the shape of a gaussian curve referred to as the vertical CH_4 production distribution (**VPD**). It starts at the depth of the SMTZ, which has been measured to be <20 cm and as shallow as <10 cm (Ketzer et al., 2024; Christian Stranne, personal communication, 2026). We assume that the CH_4 production peaks somewhere below the SMTZ, and then regresses. The CH_4 production module is setup using the following equation:

$$W(z) = e^{\left(-1/2\left(\frac{z-z_c}{\sigma}\right)\right)^2} \quad \textbf{(1)}$$

Where $z_c = \frac{(Z_1+Z_2)}{2}$ describes the center of production and $\sigma = \frac{(Z_1-Z_2)}{6}$ is the standard deviation. Outside of the interval $[Z_1, Z_2]$ the production was set to 0. The gaussian distribution was normalized such that the production when integrated equals a flux **Q**. The final production could then be described as

$$S(z) = Q \cdot \frac{w(z)}{\Sigma w(z)} \quad \textbf{(2)}$$

Where $S(z)$ is the methane production at any depth z in $kgm^{-3}s^{-1}$, and **Q** is the total methane production integrated over the depth in $kgm^{-2}s^{-1}$. During model tuning, the source that gives the flux close to our observations was **Q** $= 1 \cdot 10^{-9}$ $kg/m^2/s$ and **VPD** of 0.1-12.5m. We do a total of 7 simulations for varying vertical CH_4 production distribution widths, and 7 with varying production rates (Figure 4).

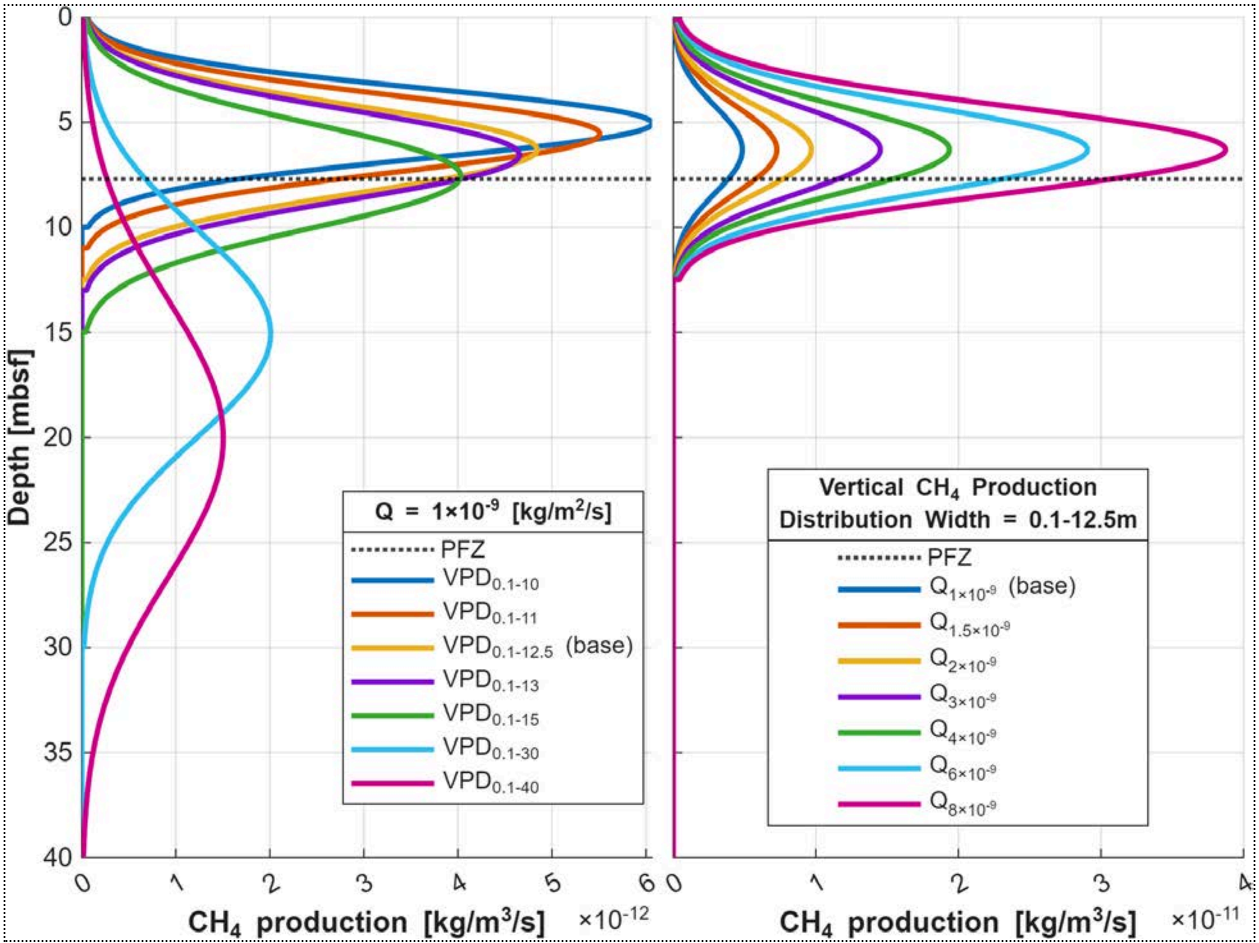

Figure 4. vertical CH_4 production distributions visualized for different simulation cases. Left: different vertical CH_4 production distribution widths with the same CH_4 production source (**Q**). Right: Different **Q** for the same vertical CH_4 production distribution width. The approximate depth of the permanently fractured zone (PFZ) for these simulations has been visually interpreted and marked with a dotted line.

5 out of the 7 **VPD** cases tested were in a relatively close range. Two of the **VPD** simulations were set up with deeper CH_4 productions as according to Egger et al., (2017) where CH_4 production from the IODP expedition hole M0063 was modeled and deemed to consist of two distinct peaks, one at 6 m and one deeper at 22 m. Our model highly simplifies this production by just having one peak, however the production rate modeled there is at least five times smaller than the one we are using here (952 μmol CH_4 / m^2 / day as opposed to our base case **Q** which, when converted to the same units, is about 5400 μmol CH_4 / m^2 / day). The study was also on a different site, and modeled on pore-water samples of trace metals and other compounds such as sulfate and iron oxides, as well as methane. Methane content in particular is often hard to observe the actual in-situ production and concentration of except for the top part of the production gradient when taking samples due to degassing, something that was reported as an issue (Flury et al., 2016; Egger et al., 2017).

3.4 Fracture module

Within each grid cell, the model calculates the pressure and assumes a fracture whenever said grid cell reaches the critical pressure, assuming the sediments to be elastic (Daigle & Dugan, 2011; Boudreau, 2012; Stranne et al., 2017; Daigle et al., 2020). When a fracture has appeared, the grid cells permeability gets set to the fracture permeability, which is usually and especially in this case a much higher permeability than the original value, permitting more gas movement vertically between grid cells. When gas moves out of the cell due to this increased mobility, the grid cells pore pressure drops, and the cell reverts back to its normal permeability value and is thus no longer considered as a fracture (Stranne et al., 2017). At a certain depth, the capillary pressure alone is enough to form fractures in the model, and as soon as the gas has reached the seafloor that top section is permanently fractured for the entire model run, referred to as the " Permanently fractured zone " and shortened to "PFZ" in this paper as per Stranne et al., (2017). The fracture permeability ($\boldsymbol{k_f}$) is set to 10^{-10} m^2 for the base case and we also do 7 cases with fracture permeabilities listed in Table 3.

Table 3. fracture permeabilities tested in simulations

$\boldsymbol{k_f}$ (m^2)	10^{-11}	5×10^{-11}	8×10^{-11}	9×10^{-11}	10^{-10} (base)	2×10^{-10}	3×10^{-10}	10^{-9}

The fracture threshold threshold ($\boldsymbol{\lambda}^*$) is a variable that corresponds to how much pressure is needed to form a fracture. If $\boldsymbol{\lambda}^* = 1$, the sediments are treated as being non cohesive and having no tensile strength, and the overpressure needed for a fracture to form is equal to the maximum principal stress (usually that is the vertical effective stress). If it is less, then it takes less pore pressure to form a fracture. For example, $\boldsymbol{\lambda}^* = 0.8$ means a fracture will occur once the pore pressure is greater than the minimum principal (often horizontal) effective stress (Daigle & Dugan, 2011; Stranne et al., 2017; Daigle et al., 2020). In the base case we have set $\boldsymbol{\lambda}^* = 1.2$, which permits some cohesion and tensile strength in the sediments, however we also analyze 7 cases in a range shown in Table 4. The sediments at the sites can be assumed to have some cohesion and tensile strength since the sediments have been determined to be mostly muddy clay, and thus the fracture threshold has to be set at > 1. In acoustic data, the free gas depth can be described to range between 5 - 9 mbsf, and our parameters were set so that the modeled PFZ for the base case would be ~7.7 mbsf. Thus the fracture threshold was tuned to 1.2, as doing so made our resulting PFZ go to 7.7m

Table 4. fracture thresholds tested in simulations.* 1.35 is outside of the realistic range, and was used for a sensitivity test.

$\boldsymbol{\lambda}$*	0.8	0.9	0.95	1	1.05	1.1	1.2 (base)	1.35*

Due to the relatively low fluxes in comparison to a site with gas hydrates, subsurface gas induced fractures are much slower compared to studies of hydrate systems, taking 10s of years instead of days. When a fracture forms, it slowly migrates upward until it reaches the permanently fractured zone where the gas then escapes the seafloor quite fast. Fractures will only form in sediments with low enough permeability (>$10^{-15.75}$m^2) (Stranne et al., 2017) and these sediments were measured to around 10^{-16}m^2, meaning the gas in these sediments should be expected to be released in a fracture dominated regime.

3.5 Simulation design

TOUGH+HYDRATE was developed to model the behaviour of hydrate bearing geologic media and flow dynamics of systems (Moridis, 2014). In the current setup, temperature and pressure are outside the ranges for possible stable gas hydrate formation. To simulate methanogenesis a function of vertical CH_4 production distribution has been introduced. A collection of scripts in MATLAB written by project supervisor and IGV Associate Professor Christian Stranne were used in order to set up the model initial states and parameters in a quick and easy fashion. Using those scripts, there are essentially three steps in modelling for this project:

- 1: Set the conditions for the system; which includes parameters such as the physical properties, vertical CH_4 production distribution width, CH_4 production source, depth of SRZ and the amount of time the simulation will take. These parameters are then spun up using an initial executive file for 10 000 years in order to establish the steady state pressure and geothermal gradient. This process is done by MATLAB scripts that read from a text file containing parameters. The script also writes this information, along with the amount of cells and the function for the Gaussian production to a new set of text files that the initial executive will read from. The initial executive output file is only two timesteps in size. After the model has been spun up, the next step can be started. The time this takes is usually around 30 seconds to 1 minute.

- 2: Running of the simulation; by which another simulation executive file is run. This file reads from the files made by the initial executive along with the Gaussian production model to simulate for a set amount of years given in the parameter text file. This process can take up to 3 hours at a time, depending on the length it simulates as well as e.g. grid cell resolution and sediment permeability. Model output is in the form of a number of ascii files for the state variables, fluxes etc.

- 3: Reading and writing fortran output files to a MATLAB data file; run by another MATLAB script in order to sort and organize every output file so that it can be interpreted easily.

When these three steps have been completed, one can easily plot for example the gas flux, permeability and gas content of the sediments for the time period that has been simulated.

3.6 Data analysis

The model outputs seafloor CH_4 gas flux in $m^3m^{-2}s^{-1}$ which is converted into mol/m^2/year. We plot the CH_4 gas flux against time from the model output time series to make the flux plots. For the sediment gas content and permeability iso-plots, we turn the model output matrices for permeability and gas content into meshgrids using the model output time series as the time component, after which we use the MATLAB “pcolor” plotting function on said meshgrid.

Frequency analysis was employed to investigate the maximum vertical resolution necessary. The idea was that the vertical resolution would impact the fracture formation, ultimately affecting the frequency of flux. For analysing the frequency, we used the MATLAB built in signal analysis toolbox. We use a Lomb-Scargle periodogram, which is a way to analyse periodic signals in unevenly sampled data, such as the time series produced in TOUGH+HYDRATE. Unlike methods such as wavelet analysis or power spectrums the Lomb-Scargle analysis is applicable on unevenly sampled data without requiring interpolation by estimating fourier power as a function of period oscillation (Lomb, 1976; Scargle, 1982; Pardo-Igúzquiza & Rodríguez-Tovar, 2013; VanderPlas et al., 2018).

3.7 Tuning for Shallow PFZ in Moat

In order to match the shallow PFZ in the so-called "moat" (right hand side in Figure 1) we tuned values for 3 different parameters: 9 grain densities ($\varrho_{[2400\ -\ 2900\ kg/m^3]}$) and two depths ($Z_{[316m\ ;\ 50m]}$) and 11 different porosities ($\boldsymbol{\Phi}_{[0.6\text{-}0.95]}$) were tested. This was merely done since they all had some impact on the depth of the PFZ.

4. Results

4.1 Matching observed flux

The parameter that controls the flux the most is the CH_4 production source as well as the vertical CH_4 production distribution width. Spreading the vertical CH_4 production distribution makes the onset of the first fluxes begin later, as well as reducing the average flux a little bit. Most likely this is due to the production being moved further down under the permanently fractured zone, since the vertical CH_4 production distribution is stretched and a larger area of production is outside of the part of the sediment with higher gas mobility. A lot of different permutations were able to generate average fluxes in the vicinity of the observed flux. They however differ in periodicity, free gas depth, time for onset of first gas flux and general amplitude of gas bursts. Different parameters had varying levels of control over these varaibles. Some of the results for the highest and lowest limit of each case is available in Table 5. Average flux was measured, for most cases, during the entire steady state window of the simulation. That would be, for example for the base case, between ~521 and 1000 years. For some of the tests, mostly the $\boldsymbol{\lambda}*$, $\boldsymbol{\Phi}$ and ϱ, the time window that the average flux was measured in is much smaller since these simulations only ran for 600 years each. The reason for this is that they were primarily used for determining the depth of the PFZ, something you don't need more than a couple of years in steady state to do. Hence the averages of those cases should be viewed with some precaution.

Table 5. Output from every simulation's highest and lowest parameter value for each case.

Case (min max) excluding base case		**Average flux (mol / m^2 / year)**		**PFZ depth (mbsf)**		**Start time of CH_4 flux (years)**		**Simulated Time (years)**	
Base case		0.98		7.7		520.9		1000	
Real world observations		**~1 to ~10**		**~5 to ~10**		-		-	
VPD $_{[0.1\ -\ 10m]}$	**VPD** $_{[0.1\ -\ 40m]}$	1.12	1.30	7.7	7.7	412.6	3012	1000	5000
Q $_{[1.5\times10^{-9}\ kg/m^2/s]}$	**Q** $_{[8\times10^{-9} kg/m^2/s]}$	1.72	14.45	7.7	7.7	351	67.9	500	500
$\mathbf{R}_{9.4\ cm}$	$\mathbf{R}_{1.97\ cm}$	1.00	0.99	7.6	7.7	523.3	519.9	1000	1000
$\boldsymbol{k_f}_{[10^{-11} m^2]}$	$\boldsymbol{k_f}_{[10^{-9} m^2]}$	0.99	1.04	7.8	7.7	536.9	511.6	1000	1000

$\lambda^*_{0.8}$	$\lambda^*_{1.35}$	1.11	0.74	9.6	6.92	515.5	543.5	600	600
$\Phi_{0.6}$	$\Phi_{0.95}$	0.98	0.95	3.6	8.98	586.7	597.7	600	600
$\varrho_{[2400\ kg/m^3]}$	$\varrho_{[2900\ kg/m^3]}$	0.97	0.71	8.62	6.3	515.9	568.8	600	600
$Z_{51\ m}$	$Z_{316.2\ m}$	0.93	0.91	8.13	7.82	71.8	395.9	100	600

4.2 Effect of methane source

When the vertical CH_4 production distribution width was increased, the general average flux in the steady state period decreased, and it took significantly longer time for the gas to escape the sediments. An increase in vertical CH_4 production distribution width from 0.1-10 to 0.1-15m saw a small but steady decrease in the average flux, and the time onset of gas escape also increased by about 50 years per meter. This relationship is only true down to a certain vertical CH_4 production distribution width, as seen in Figure 5. When a large enough portion of the gas production is underneath the PFZ, fractures take more time to build up resulting in larger bursts of methane being released and long times of almost no flux at all.

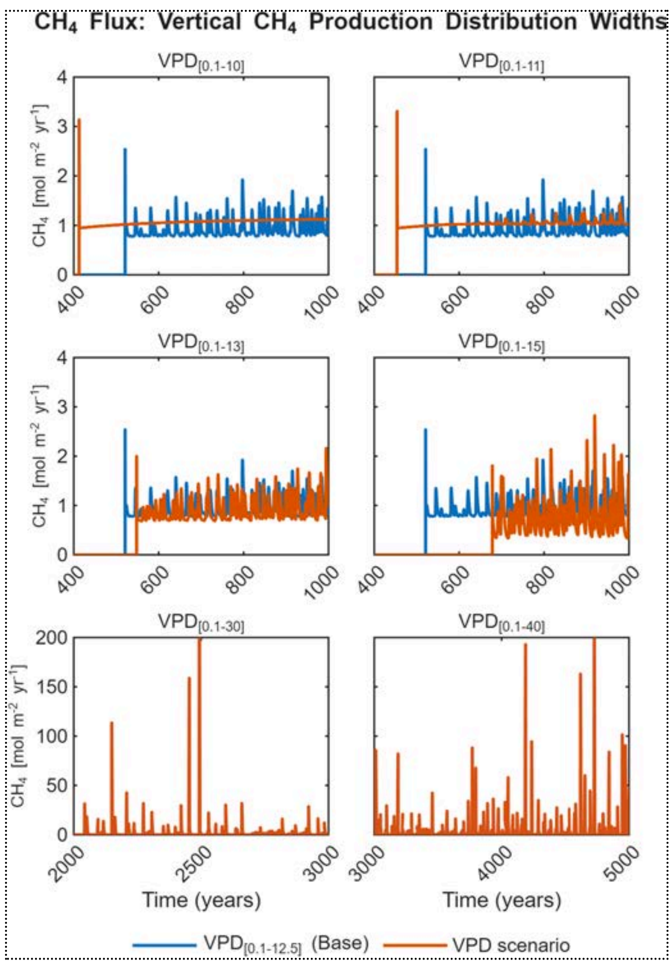

Figure 5. Comparing CH_4 gas fluxes for the base case (**VPD**$_{[0.1\text{-}12.5\ m]}$) to **VPD**$_{[0.1\ -\ 10m\ —\ 0.1\text{-}40m]}$. Note that the time for onset of gas release, as well as the ranges for CH_4 gas flux for **VPD**$_{[0.1\text{-}30\ ;\ 0.1\text{-}40m]}$ were too great for the base case gas flux to be on the same plot.

The most significant change in average flux came from altering the rate of CH_4 production (Figure 6). It also greatly decreased the amount of time it took for the gas to reach the surface. When increasing the CH_4 production source sevenfold, the average flux increases by one order of magnitude (from ~1 to ~14 mol/m^2/year) while the time for gas escape to onset decreased from 515 to 67 years, as shown earlier in the summary (Table 5).

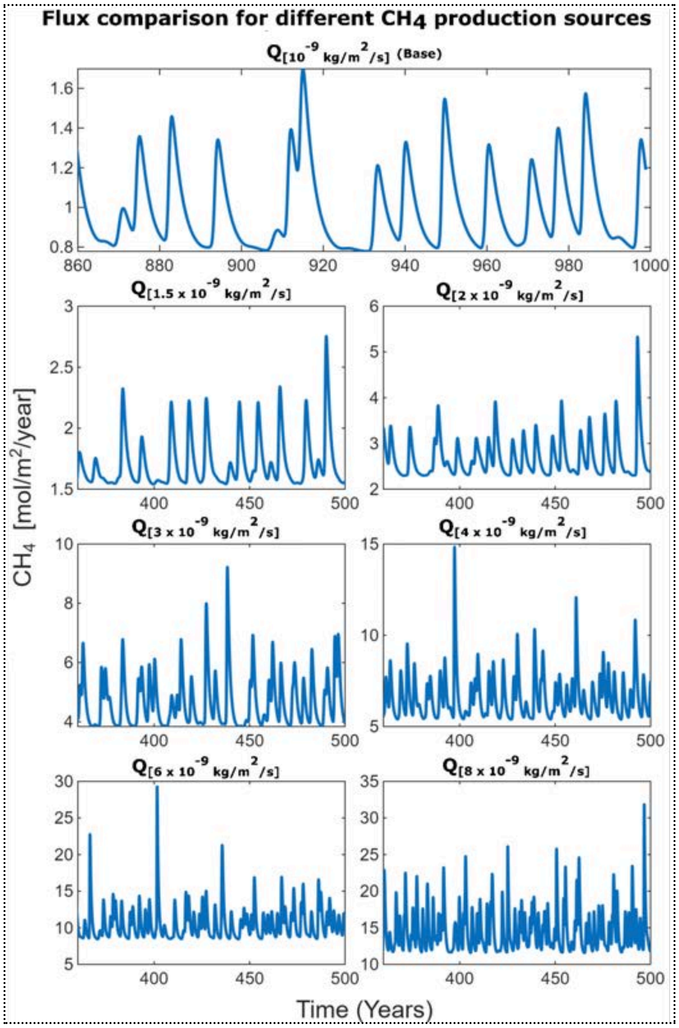

Figure 6. CH_4 gas flux in a 150 year timespan for different CH_4 production sources (**Q**). Note that the Y axes have been adjusted in accordance to the flux. For the base case the time window is set to 850-1000 years, for the other simulations it is set for 350 - 500 years since the onset of first gas escape for the base case is >500 years, and the other simulations only 500 years were simulated since that was a sufficient time window. The time window still captures the system in steady states.

4.3 Effect of fractures

To understand how methane transport is influenced by hydraulic fractures, it is useful to see how fracture propagation manifests in the model. Figure 7 compares the base case with **VPD**$_{[0.1\text{-}30m]}$ and shows the evolution of gas content in the sediments over time, along with sediment permeability and CH_4 gas flux. In both cases, when analysing the gas content of the sediments, fracture flow is visible. One can trace a pocket of gas from the methanogenic zone, up through the PFZ and out from the seafloor, manifesting as a burst in CH_4 gas flux (Figure 7A and B). If one looks at the lowermost plot (Figure 7C) the fracture propagation manifests as narrow bands of high permeability in otherwise low permeability media, growing upward from the CH_4 saturated sediments joining the PFZ. The two **VPD** cases also show how the relative position of methane production to the PFZ affects fracture and flux dynamics. In the deeper **VPD**$_{[0.1\text{-}30m]}$ case, gas accumulates over a larger depth interval and releases larger packets of gas, with periods of zero flux. The base case on the other hand has a shallower production, of which some part escapes through fractures, while some escapes constantly in a seeping manner. Moreover, it is also visible that the propagation of fractures in this system takes years. In Stranne et al., (2017), where the Fracture module was first introduced, the fractures propagate on a timescale of days to weeks. This is because in that study the system being modeled had gas hydrates and thus the flux is many orders of magnitude higher than in this study.

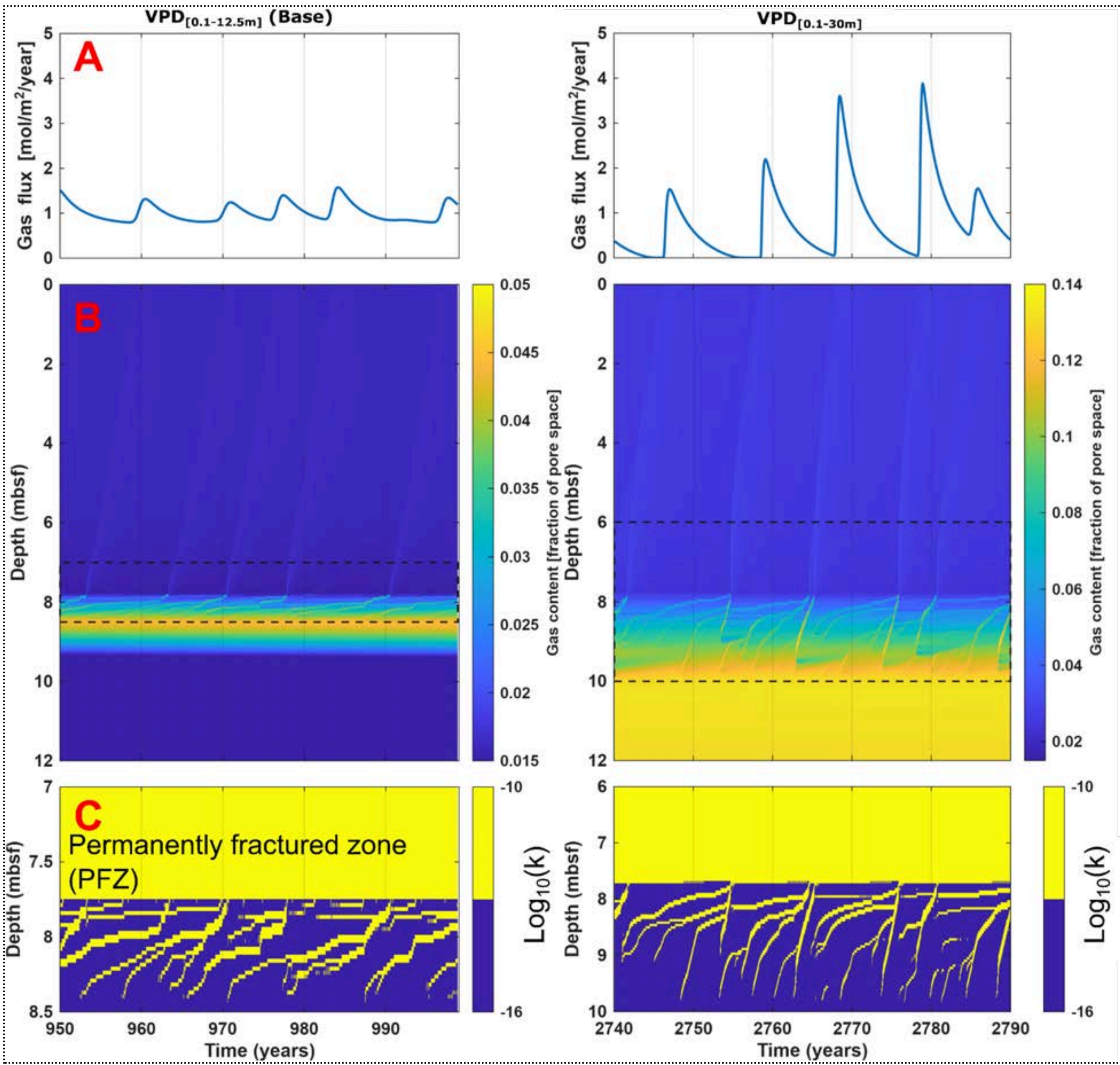

Figure 7. **A**: CH_4 gas flux for base case (**VPD**$_{[0.1\text{-}12.5m]}$) (left) and **VPD**$_{[0.1\text{-}30\ m]}$ (right). **B**: Gas content in sediments vs depth and time. **C**: Permeability in sediments over depth and time. Note the difference in scale of gas content colour bar, as well as the different extents of the depth axis for **C**, which the dashed rectangle in **B** indicates.

As explained, fracture propagation coincides with the spikes in CH_4 flux. Depending on modelling parameters such as $\boldsymbol{\lambda}^*$, ϱ and $\mathbf{Q}$, the fractures propagate at different speeds. The fracture threshold ($\boldsymbol{\lambda}^*$) affected the PFZ and thus the simulations using smaller $\boldsymbol{\lambda}^*$ were all less fluctuating than the base case. This correlation can be seen in Figure 8. There is a clear transition after $\boldsymbol{\lambda}^*$ goes above 1, where the fracture dominated flow starts. An increasing fracture threshold results in an upward migration of the PFZ. In Figure 8, the small wobble at the end of the top right graph for case $\boldsymbol{\lambda}^*{}_1$ suggests a larger burst of gas in the coming years is imminent, and thus that the system in neither of the low $\boldsymbol{\lambda}^*$ simulations ever reached steady state in 1000 years. fractures start to propagate near the end of the simulation, correlating with the small bursts in gas flux. For cases $\boldsymbol{\lambda}^*{}_{[\leq 0.95]}$ the PFZ was migrating downward still before the simulation had ended. $\boldsymbol{\lambda}^*$ had a small effect on the onset time for gas release, the largest difference being $\boldsymbol{\lambda}^*_{[1.15 - 1.2]}$ going from ~517 years to ~520 years. Cases $\boldsymbol{\lambda}^*{}_{[<1.15]}$ had roughly the same time for gas release at ~515 years.

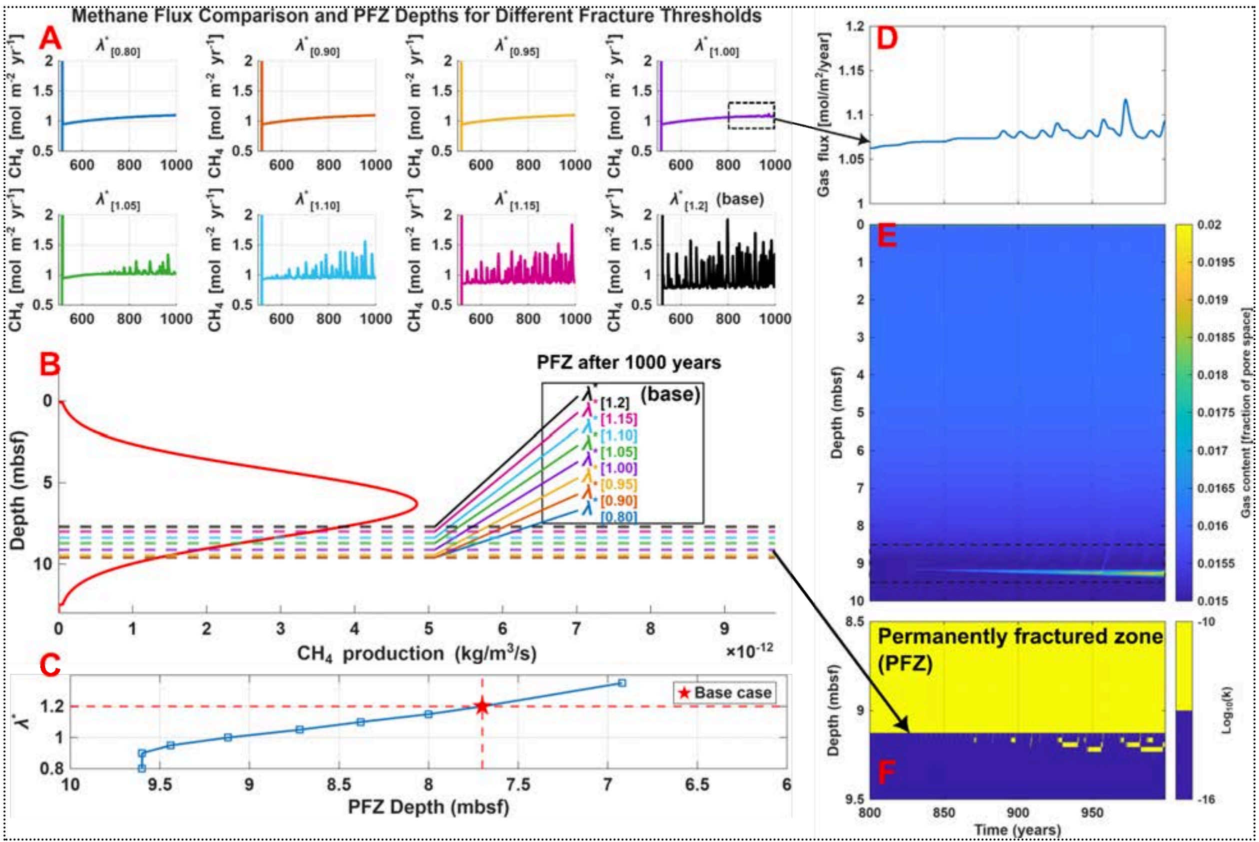

Figure 8. Comparing the fluxes and PFZ depths of different fracture thresholds. **A**: CH_4 gas flux against time for $\boldsymbol{\lambda}^*{}_{[0.8 - 1.2]}$ starting at 500 years. **B**: dotted lines show PFZ after 1000 years, which for cases $\boldsymbol{\lambda}^*{}_{[>0.95]}$ constitutes a steady state. Solid red line shows vertical CH_4 production distribution. **C**: PFZ depth after 1000 years for every $\boldsymbol{\lambda}^*$ against $\boldsymbol{\lambda}^*$ with base case marked. **D**: CH_4 gas flux for $\boldsymbol{\lambda}^*_1$ starting at 800 years. **E and F**: permeability and gas content plot for $\boldsymbol{\lambda}^*_1$.

With this established, the influence of fracture permeability ($\boldsymbol{k_f}$) can be examined. $\boldsymbol{k_f}$ describes how fast, and how much methane can migrate through hydraulic fractures. As a result of this, $\boldsymbol{k_f}$ affects the onset time for gas escape (Figure 9), with onset time increasing with lower permeabilities.

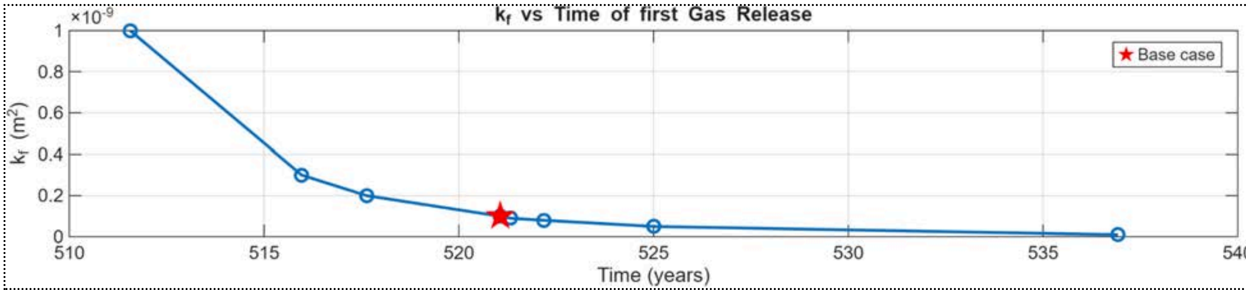

Figure 9. time for first gas release measured for $\boldsymbol{k}_{f[10^{-9}-\ 10^{-11}m^2]}$

Fracture permeability also affects the size of the first burst of gas that the system experiences. Cases $\boldsymbol{k_f}$ $_{[<\ 10^{-10}m^2]}$ had lower spikes of gas flux at the first onset of release than the base case, while cases $\boldsymbol{k_f}$ $_{[\ >\ 10^{-10}m^2]}$ all had higher breakthrough fluxes. Presumably, this is down to the migration speed of CH_4 in the fractures, with lower permeabilities limiting the gasses movement and forcing it to seep out slowly rather than bursting. Other than that, $\boldsymbol{k_f}$ values in close range of the base case ($\boldsymbol{k_f}$ $_{[8x10^{-11};\ 9x10^{-11};\ 2x10^{-10}m^2]}$) do not affect the flux profile to any large extent, as seen in Figure 10. There are some differences to note when examining the lowest and highest $\boldsymbol{k_f}$ simulated, mainly the onset time as mentioned earlier, but also the perceived periodicity, with $\boldsymbol{k_f}_{[10^{-9}m^2]}$ having larger amplitude and higher frequencies in its flux profile when compared to $\boldsymbol{k_f}_{[10^{-11}m^2]}$.

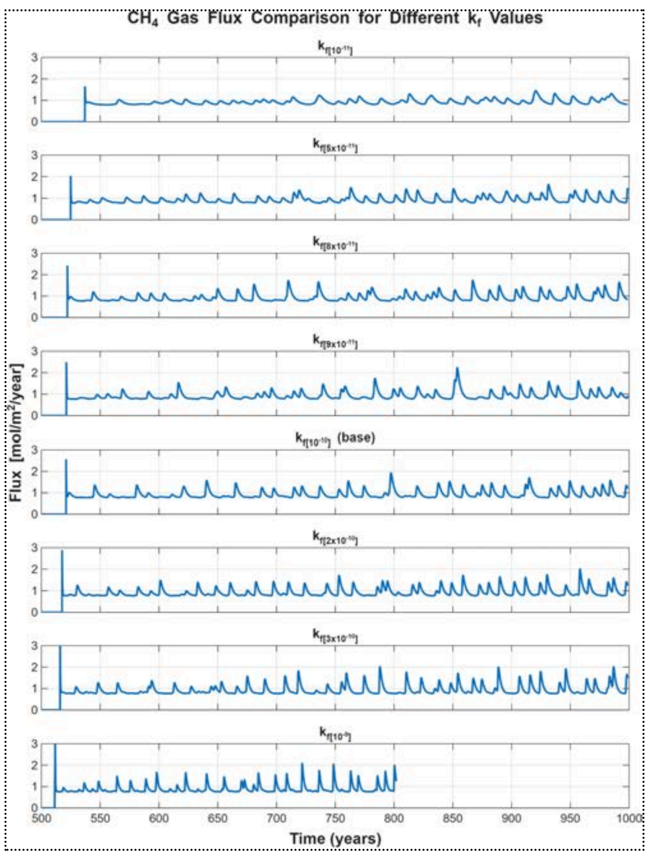

Figure 10. CH_4 gas flux vs time for different $\boldsymbol{k_f}$ simulations. Note that the $\boldsymbol{k}_{f[10^{-9}m^2]}$ simulation only could run for 800 years maximum due to model limitations.

The higher $\boldsymbol{k_f}$ simulations gave sharper spikes in gas release compared to the lower $\boldsymbol{k_f}$ cases, the lowest $\boldsymbol{k_f}$ case ($\boldsymbol{k_{f\ [10^{-11} m^2]}}$) had the lowest amplitude in flux bursts, sediments were more saturated in CH_4, and gas propagated slower in the PFZ while the fractures themselves propagated at the same speed, something visible in Figure 11. This means that less permeable fractures lead to slower gas propagation in the PFZ, leaving the PFZ more saturated than in cases with higher $\boldsymbol{k_f}$, such as the base case.

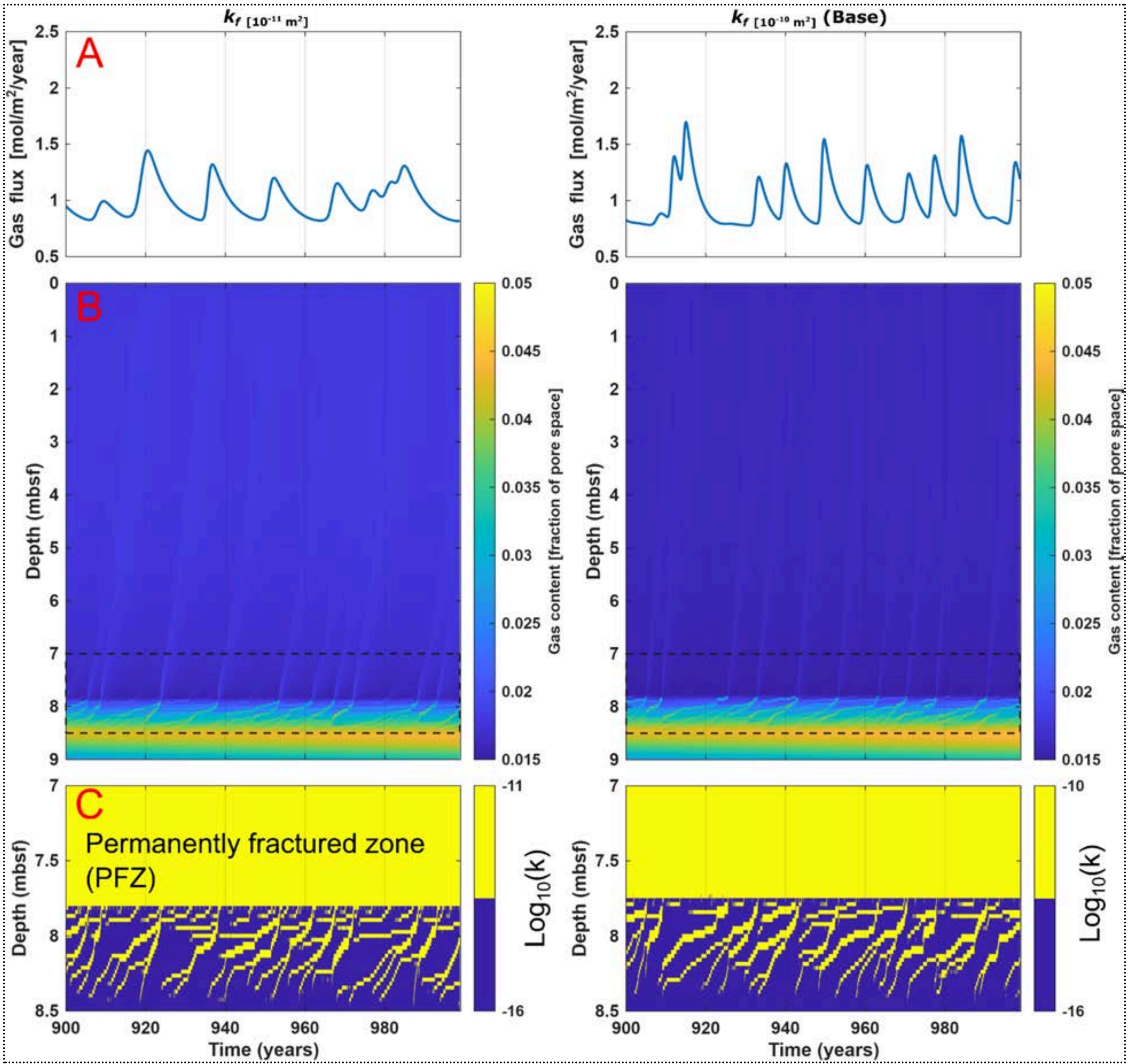

Figure 11. **A**: CH_4 gas flux for $\boldsymbol{k_{f[10^{-11} m^2]}}$ (left) and base case ($\boldsymbol{k_{f\ [10^{-10} m^2]}}$) (right). **B and C**: Gas content and permeability in sediments. Black dashed rectangle in **B** indicates depth limits for **C**. The Figure captures a 100 year time window between 900 and 1000 years.

4.4 Resolution tests

Increasing resolution concentrates the peaks to 0-20 year period ranges, while the lowest resolution used ($\mathbf{R}_{9.4\ cm}$) spreads out the distribution of peaks. The difference in file size and simulation time between the base case and the higher resolution simulations were large, while the resulting differences were not really significant. Therefore we stuck with the base case resolution ($\mathbf{R}_{2.64\ cm}$) for the other simulations. The periodogram shows that most of the peaks have a period of ~17-28 years, with the higher frequency peaks with periods of around 9 years for cases $\mathbf{R}_{[<1.97\ cm]}$. The highest resolution cases were generally skewed toward high frequencies (Figure 12).

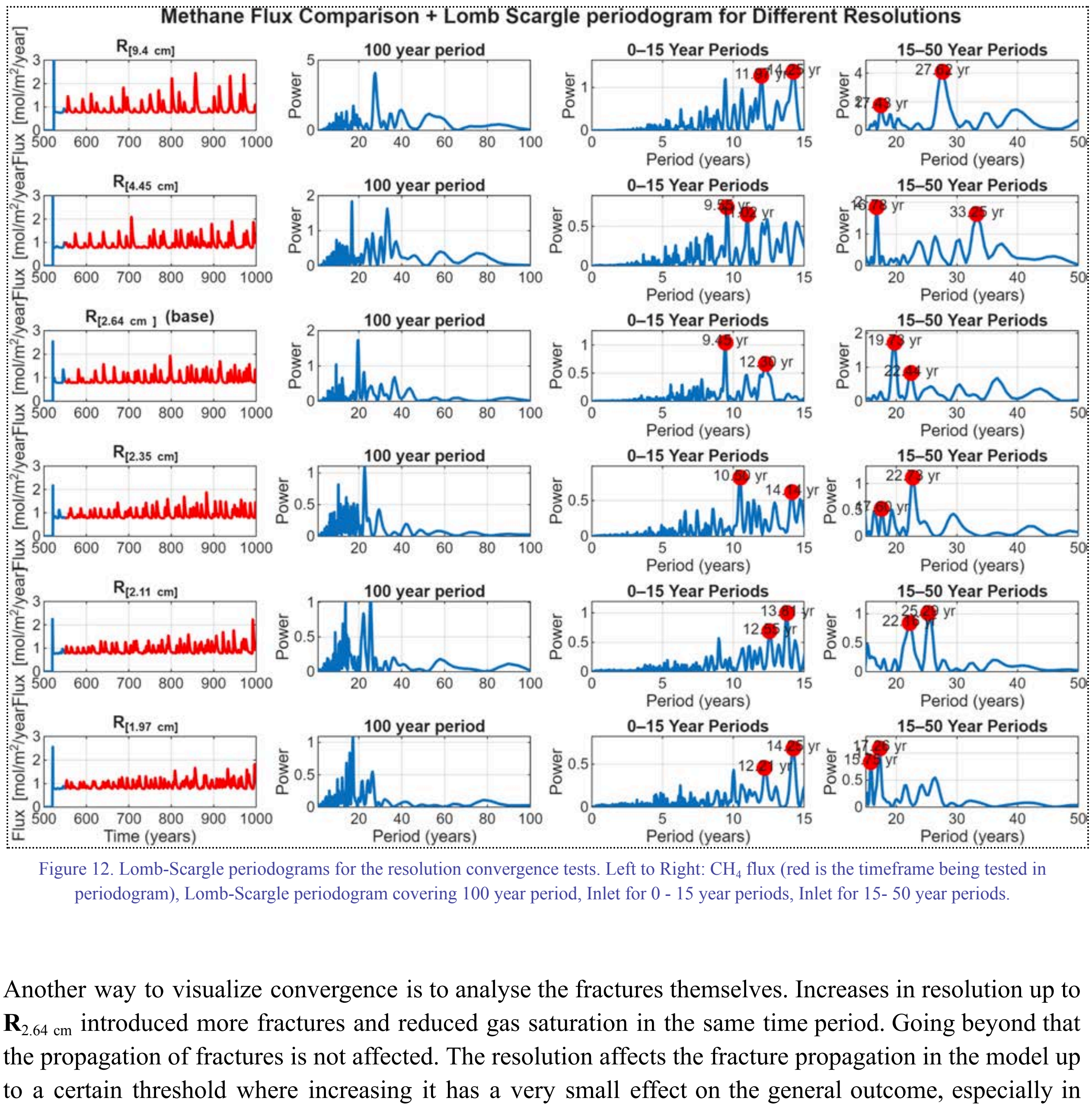

Figure 12. Lomb-Scargle periodograms for the resolution convergence tests. Left to Right: CH_4 flux (red is the timeframe being tested in periodogram), Lomb-Scargle periodogram covering 100 year period, Inlet for 0 - 15 year periods, Inlet for 15- 50 year periods.

Another way to visualize convergence is to analyse the fractures themselves. Increases in resolution up to $\mathbf{R}_{2.64\ cm}$ introduced more fractures and reduced gas saturation in the same time period. Going beyond that the propagation of fractures is not affected. The resolution affects the fracture propagation in the model up to a certain threshold where increasing it has a very small effect on the general outcome, especially in fracture propagation, but the file sizes and time it takes to run the simulations increase drastically (Figure 13).

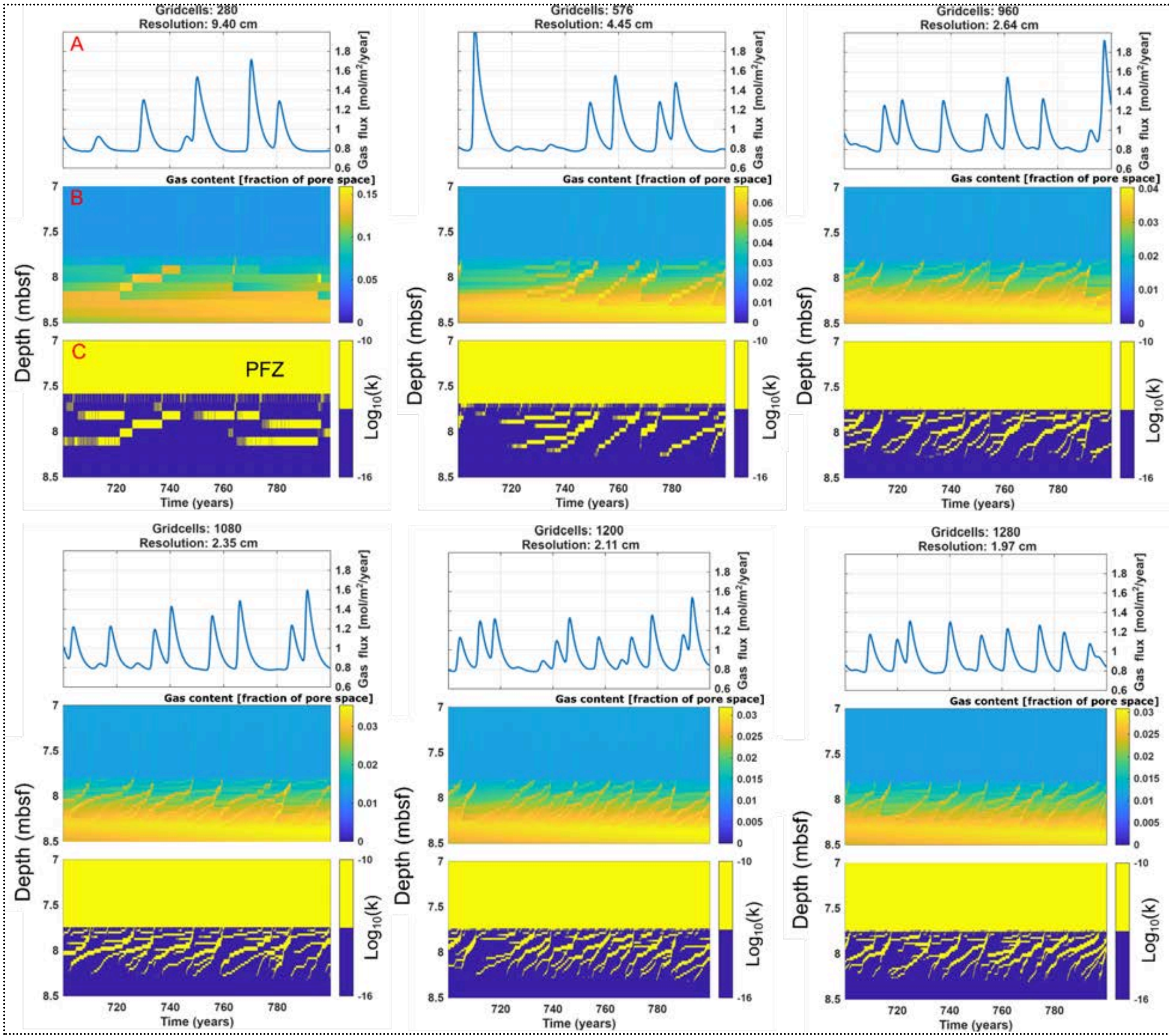

Figure 13. Flux, gas content and permeability plots for different simulation resolutions. **A**: CH_4 gas flux vs time. **B**: Gas content in sediments vs depth and time. **C**: Permeability in sediments vs depth and time. Note the differences in scales for the gas content color bar.

4.5 PFZ depth controls

4.5.1 Fracture Threshold

The fracture threshold (λ^*) can be thought of as a function of the sediment cohesion and tensile strength (Stranne et al., 2017). At first we tested 7 different fracture thresholds, which led to discovering a link between the parameter and the PFZ depth. In order to reduce the PFZ depth to 5 mbsf to match the so-called "moat" (right hand side in Figure 2 and 16) we increased the λ^* testing range (0.8 - 1.2), however the increase necessary in order to produce a shallower PFZ quickly fell outside of any realistic value, without making the PFZ shallow enough. Hence, other physical properties with more realistic ranges were deemed to be more appropriate. Every PFZ and λ^* is shown in Figure 14A.

4.5.2 Porosity

Porosity (Φ) tests ranging from [0.6 - 0.95] (Figure 14B) show that the depth of the PFZ is highly sensitive to small changes in porosity. It can reproduce the observed ~5 mbsf PFZ interpreted in the moat, requiring a lower porosity of ~0.7. Silty Baltic sea sediments can range in porosity from 0.6-0.75 while more muddy sediments will be more porous, typically ranging from 0.75-0.9 (Lipka et al., 2018).

4.5.3 Grain Density

In order to avoid unrealistic fracture thresholds when trying to match the acoustic data, we also tuned the sediment grain density (ϱ) between [2400 - 2900] kg/m^3 (Figure 14C), however these tests were not able to recreate the observed PFZ depth in the moat (~5 mbsf) as it would require densities above ~ 3000 kg/m^3.

4.5.4 Water Depth

To investigate if the observed differences of the PFZ depths over the EK80 line, including the 5 mbsf at the moat, we performed three depth controls to see if the small differences in water depth (**Z**) could be a reason. The moat is about 15 meters deeper than the shallowest part of the site. Our results show a slight deepening of the PFZ when the water depth is shallower, however it is not a powerful enough trend to be the only factor. Comparing modeled water depths (**Z**) of 418m, 316m and 50m, the PFZ deepens around 20cm for every 100 meters in a linear fashion (Figure 14D).

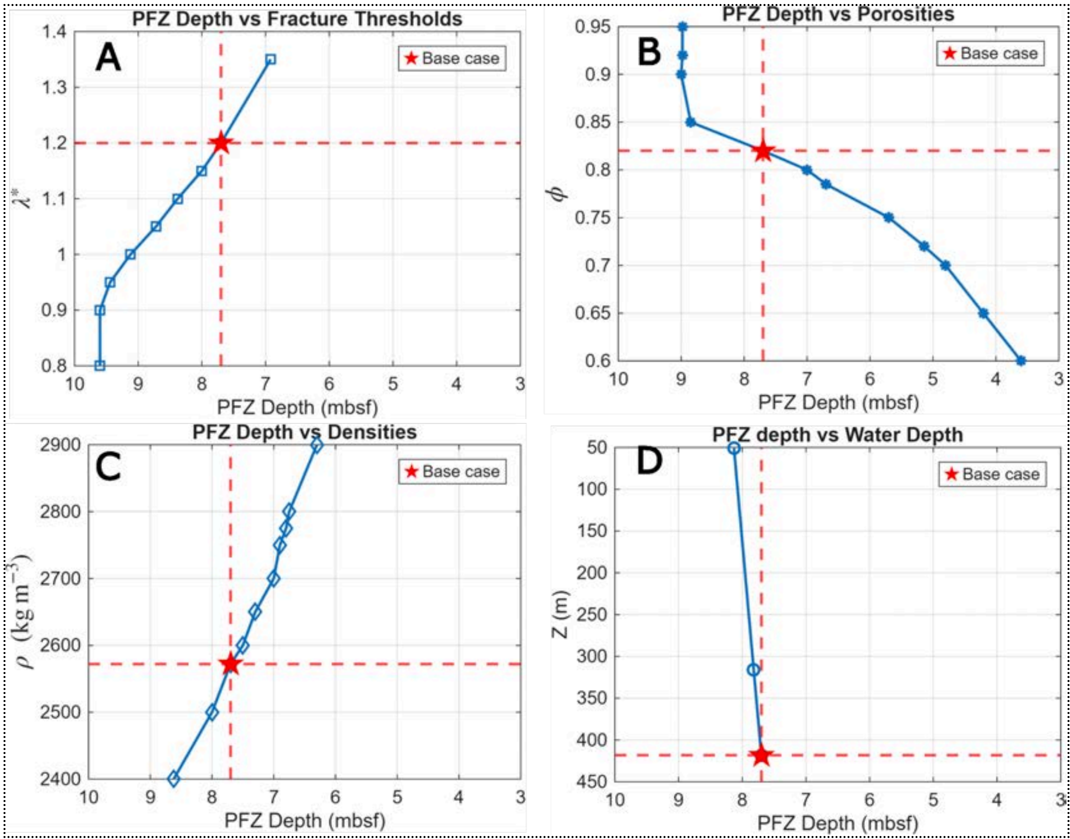

Figure 14. PFZ depth control tests on four different parameters ($\boldsymbol{\lambda^*}$, $\boldsymbol{\Phi}$, ϱ and Z).

5. Discussion

5.1 Controls on seepage

The simulations suggest that the dominant control on methane seepage behaviour is the relative position between the methane production distribution and the PFZ. A flowchart depicting a simplification of the general paths of influence for the different parameters and outcomes discussed here, can be seen in Figure 15.

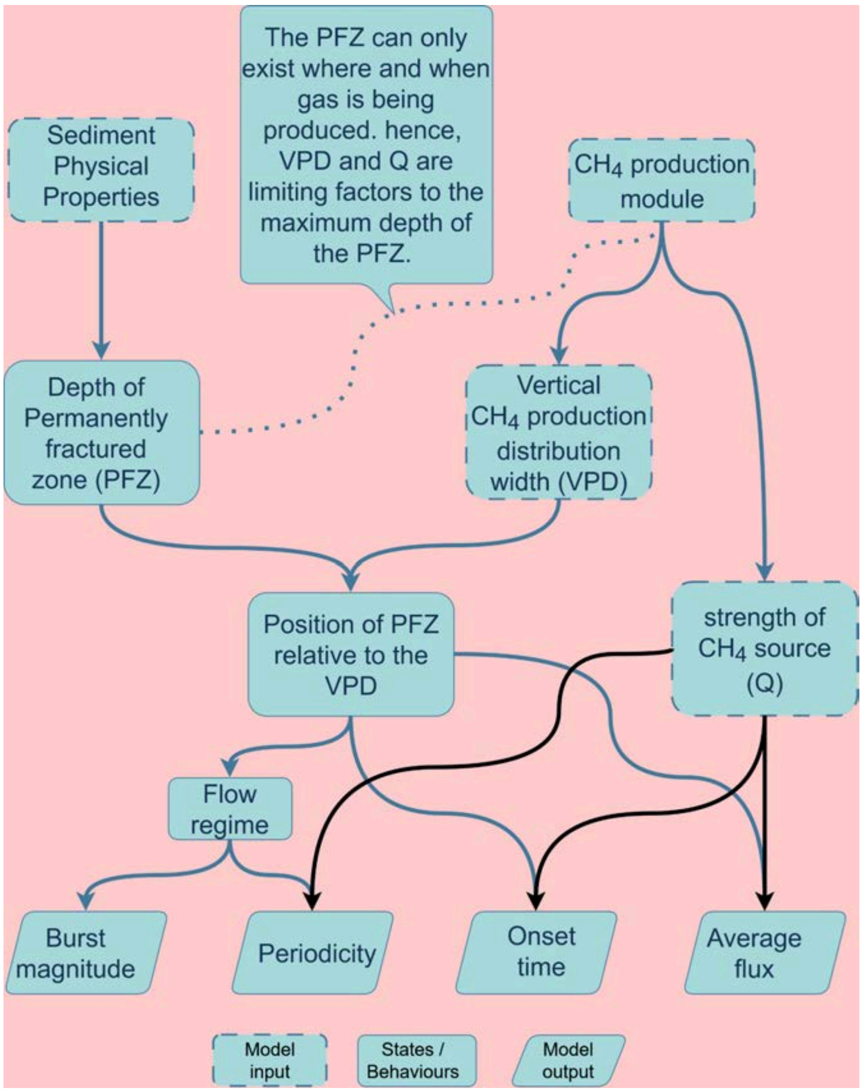

Figure 15. flowchart detailing the impact different model inputs have on states and output

Multiple parameter combinations were able to reproduce observations. Therefore, the base case should not be seen as a unique solution, but as one of many plausible ones. There are still uncertainties regarding the periodicities in the real life seepage. The goal from the start was to perform in detail frequency analysis on the flux data for different parameters, however it was determined that the periodicities that were found were not relevant to our research. The periodicity in the model output is on the timescale of years to 10s of years, which are timescales that we do not have data for at this time. The periodicity we were looking for would be mostly in the timescale of months to weeks, and the signal is too uncertain to discern any frequency that high.

Some frequency analysis was still performed on the vertical resolution tests, because it is clear that the vertical resolution has an impact on the fracture dynamics. The periodogram for the vertical resolution tests do identify recurring peaks for multiple resolutions, mostly in the 10 and 20 year range. When increasing the resolution beyond $\mathbf{R}_{2.64\ cm}$, the periodograms look very similar as the long term periods decrease. Other parameters, such as **Q**, and $\boldsymbol{k_f}$ also affected frequency of fluxes, something that can be observed from the flux data. Faster moving fractures, induced by either a higher source of methane or more permeable fractures tend to make the signal more periodic in nature, with higher amplitude and shorter wavelengths.

Should these results accurately represent real life conditions, then if if taken into account the observed free gas depths ranging from ~5m to ~9m at most, an average flux of ~1 mol CH_4 / m^2 / year as well as the observed (but not entirely quantified) periodicity the most realistic simulation cases would be those that have a production that peaks somewhere inside the PFZ but still have enough production below the PFZ to cause fracturing that is noticeable in flux measurements. This would translate to a methanogenic zone peaking in production somewhere between 6-7.5 mbsf, a PFZ edge at ~7.7 mbsf and a CH_4 production of ~10^{-9} kg / m^3 / s. This encapsulates the base case, but also some deeper production peaks / wider vertical CH_4 production distributions, such as cases $\mathbf{VPD}_{[0.1\text{-}13\ ;\ 0.1\text{-}15m]}$ where the average fluxes were a bit lower and the peaks a bit higher. Due to the large area of the study site, and the likely spatial variability of properties such as grain density, cohesion and tensile strength, multiple simulated cases can be reflective of real conditions. As shown in our results, small differences in porosity, sediment grain density, cohesion and tensile strength have been shown to be a sensitive control on the depth of the PFZ. Points A and B in Figure 16 can be assumed to have porosities above 85%, while C and D seem to be less porous, landing between 80 and 85%, with the shallowest PFZ (~5m in the moat) can be assumed to have a porosity of about 70-75%. This would suggest more silt and higher densities eastward in the Figure, with more porous, more cohesive, muddier and less dense sediments, possibly more organic material westward. The PFZ is highly sensitive to $\boldsymbol{\Phi}$ when the $\boldsymbol{\Phi}$ range is <85%. Above that it makes very little difference. The same relationship is true for the $\boldsymbol{\varrho}$ cases, the PFZ would not go beyond ~9mbsf. This suggests that, at a certain point, the PFZ depth is limited by the production rate of methane (**Q**) and the **VPD**.

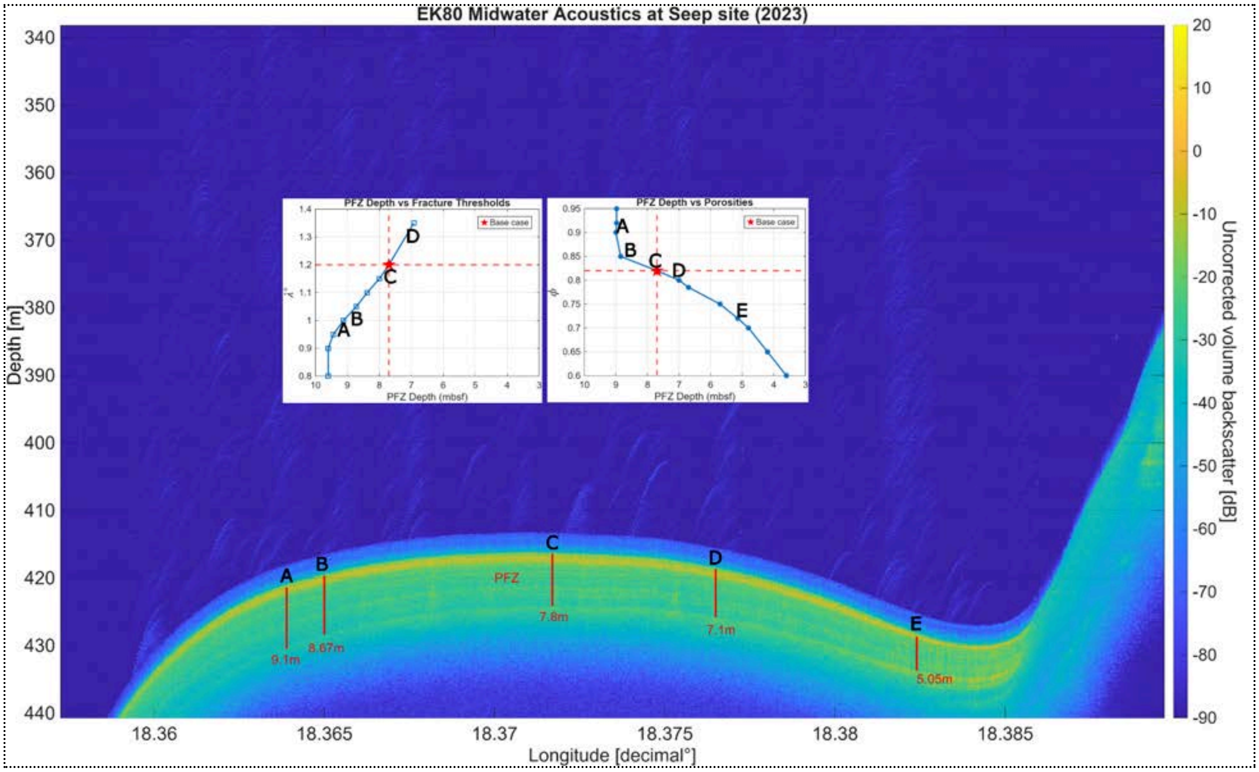

Figure 16. Interpretation of Simrad EK80 midwater acoustic data from the active seep site. The permanently fractured zone has been visually interpreted with red lines at five different locations (A, B, C, D & E) with their respective PFZ depth mapped on physical properties.

The biggest control on CH_4 gas flux simulated in TOUGH+HYDRATE using these parameters is here shown to be the CH_4 production source (**Q**), with vertical CH_4 production distribution width (**VPD**) slightly after. When modeled to greater depths, the CH_4 gas flux is not at all realistic, since we see bursts of gas escape to several orders of magnitude higher than what is observed in real life. The average flux is still realistic, but not the way it is being released. Had this been the case we would not see a continuous release of CH_4 but gas blowouts every other year, which we do not. The biggest control on the time it takes for gas to start leaking is the **VPD**, while the biggest control on flux irregularity were both **Q** and **λ***. The latter determines the depth of the PFZ more so than any other parameter that was tested. It should come as no surprise that a larger production rate in the sediments ultimately lead to a higher average flux when running the simulations.

During simulation runs, we developed a system for describing certain behaviours of the flux profile, coupled with the relative depth of the PFZ to the **VPD**. We describe three different flow regimes that were present, all dependent on the relative depth of the PFZ to the **VPD**.

The first one is constant CH_4 seepage, which occurs if the **VPD** sits almost entirely inside of the PFZ, meaning the CH_4 does not build up and burst through fractures episodically, but migrate upward through the PFZ in a constant seepage. The second one is mixed and occurs when, as in most of the simulations, there is a significant enough part of the **VPD** that sits underneath the PFZ. If such is the case, pockets of gas will slowly build up underneath the PFZ until a certain pressure threshold is surpassed, a fracture forms, and the gas moves upward. Most of the simulations behave like this, with some background seepage still ongoing because of the fact that methanogenesis is still also taking place inside of the PFZ.

The third flow regime occurs when the CH_4 escapes solely through fracture flow. This happens when the vast majority of the **VPD** sits beneath the PFZ. Then, the same build up of pressure and release as described occurs, but with little to no background seepage at all. Because the flow regime dictates the flux and the way the methane is being released, the flow regime ultimately affects the frequency of fluxes. This relationship is illustrated in Figure 17.

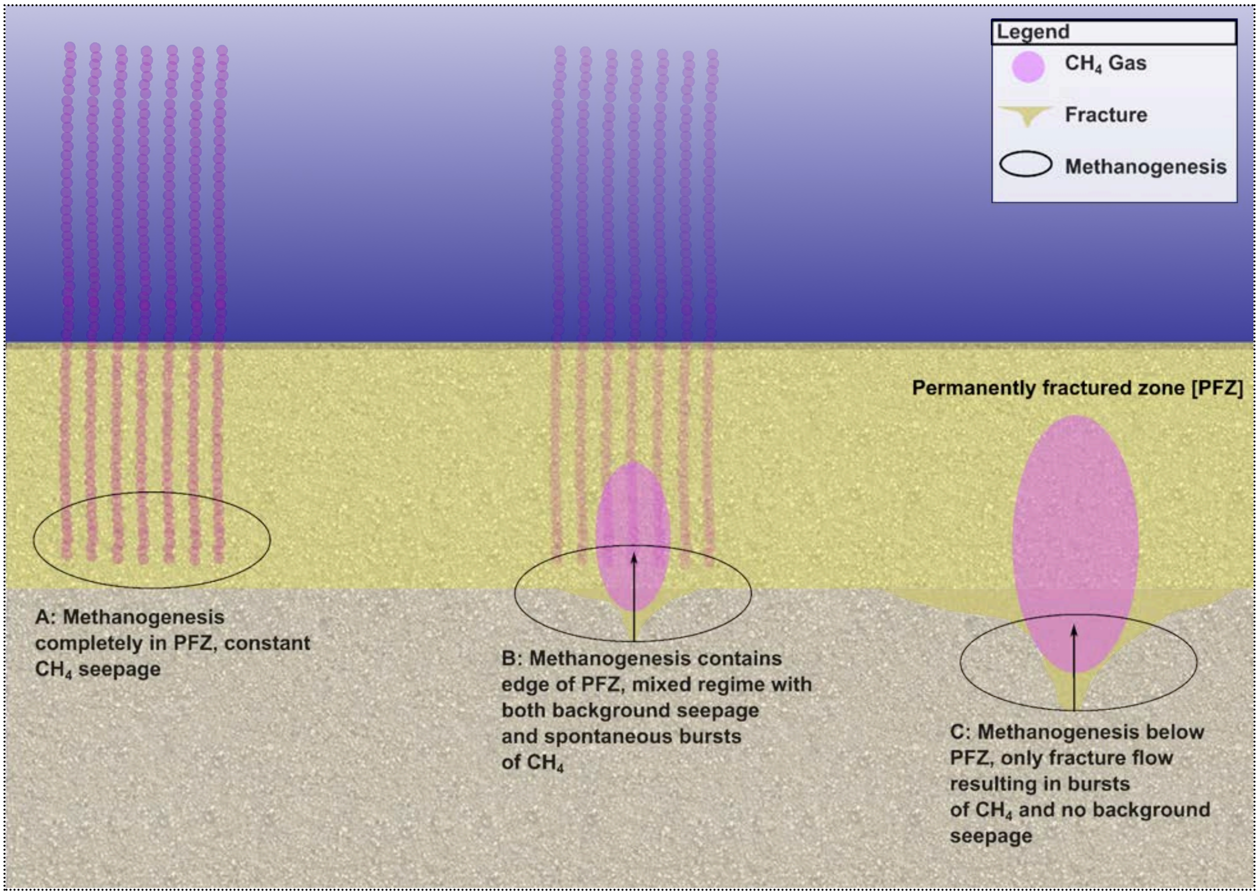

Figure 17. Qualitative illustration of three different flow regimes observed in model runs. **A**: Constant seepage; very little to zero periodicity in flux profile. includes cases $\boldsymbol{\lambda^*}_{[<1]}$ and $\mathbf{VPD}_{[0.1\text{-}10m]}$. **B**: Mixed flow regime; some background seepage and also fracture induced periodicity in flux profile. includes most of the cases observed (The base case, $\boldsymbol{\lambda^*}_{[>1]}$, every $\boldsymbol{k_f}$ case and $\mathbf{VPD}_{[0.1\text{-}11;\ 0.1\text{-}12.5;\ 0.1\text{-}13;\ 0.1\text{-}15m]}$). **C**: Fracture dominated regime; highly periodic flux profile with large bursts of methane interlaced between periods of almost no flux. observed in cases $VPD_{[0.1\text{-}30\ ;\ 0.1\text{-}40m]}$. The cyclic accumulation and release that both **B and A** show is consistent with conceptual models regarding gas bubble rise behavior and fracture propagation in marine sediments (Boudreau, 2012; Stranne et al., 2017; Daigle et al., 2020).

Stranne et al., (2017) found that changes of $\boldsymbol{k_f}$ and $\boldsymbol{\lambda}^*$ did not affect the model output a lot except for when the sediment permeability was set to $10^{-15.75}$ m^2. The results in these simulations lean toward the same conclusions regarding $\boldsymbol{k_f}$, however, there are some differences to note here. Changes in $\boldsymbol{k_f}$ did not really have any larger effect (except the lowest value used ($10^{-11}m^2$) which saturated the free gas zone somewhat more than the other cases) on the saturation of the PFZ, fracture propagation or average flux, however it did affect the onset time for the gas release, with lower $\boldsymbol{k_f}$ values slightly reducing the onset time, as well as having sharper (shorter in time and larger in amplitude) flux spikes. Increasing the $\boldsymbol{k_f}$ values seemed to have a similar effect to what the increased resolutions had regarding the frequency of fluxes. Changes in

λ^* greatly affected the modelling results, especially the depth of the PFZ, which in turn led to a longer time for fracture flow to begin, even though gas had at first been released in a seeping manner.

Notably, in case λ^*_{1}, at the very end of the simulation some periodicity is introduced to the flux. When looking at the permeability plot for this case, it is clear that fractures actually start to form at the very end of the simulation, and also that there is an increase in gas content in the regular permeability sediments just below the PFZ, which then suggests that this is also the case for cases $\lambda^*_{[<1]}$. When looking at case $\lambda^*_{1.05}$ for example, we can still deduce that these fractures and subsequent bursts of gas will be very small. This suggests that the very edges of the methane production curve eventually reaches overpressure in the lower permeability part of the sediments and if that is the case, it means that those simulations did in fact not reach a steady state in the 1000 years simulated. This means that for cases $\lambda^*_{[<1]}$ it takes >1000 years for the system to reach steady state. In the base case, despite CH_4 being produced down to 12.5m, fractures only appear beneath the PFZ until around 8.3 mbsf (Figure 7). This suggests that at the tail ends of the gaussian function, not enough pore pressure is being generated from the methanogenesis, and either the CH_4 produced beyond this depth is only moving upward through diffusive processes or it is trapped in the sediments until the pressure is high enough, as suggested earlier for λ^*_{1}. We can compare this to **VPD**$_{[0.1\text{-}30\ ;\ 0.1\text{-}40m]}$. The fractures for both these cases seem to start propagating at the same depth, however the gas is saturated way deeper in case **VPD**$_{[0.1\text{-}40m]}$ (Figure 18).

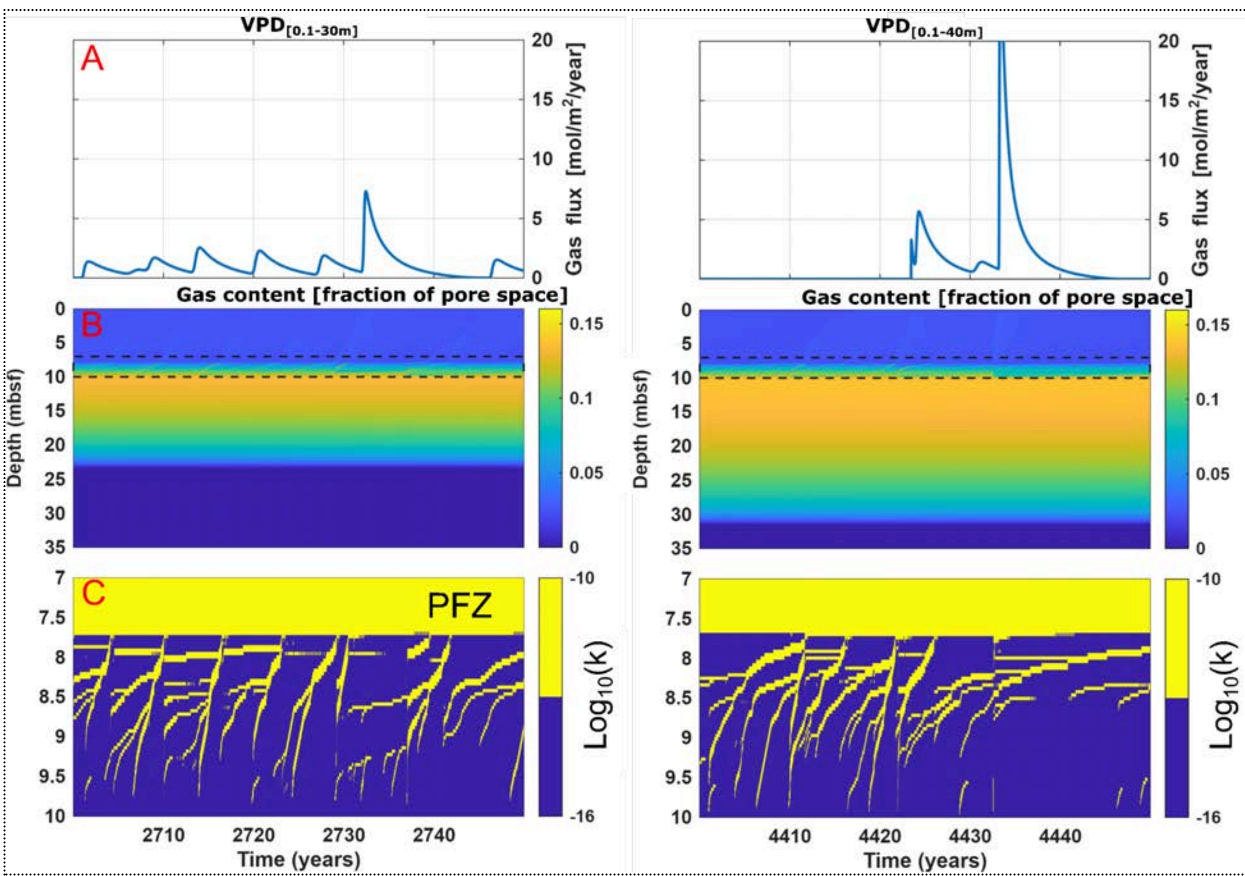

Figure 18. Flux, gas content and permeability plots for cases **VPD**$_{[0.1\text{-}30;\ 0.1\text{-}40m]}$. **A**: CH_4 gas flux vs time. **B**: Gas content in sediments vs depth and time. **C**: Permeability in sediments vs depth and time. Black square in **B** indicates depth limits for **C**.

The bursts found in the **VPD**$_{[0.1\text{-}30\ ;\ 0.1\text{-}40m]}$ appear inconsistent with current observations, since the bursts exceed well over 100 mol / m^2 / year at times. To combat this one could try a much lower source at this depth, but then the flux would be greatly reduced and the onset for gas escape would increase dramatically. This is unrealistic since the methane producing sediments are only about 9-7 thousand years old (Egger et al., 2017) and seeing how much small changes in the source affects the time for gas escape onset, setting the source low enough for reducing the bursts would, even if we discount the average general flux reduction, also extend the time beyond what is deemed to be realistic.

The average flux for both simulations with deeper sources (**VPD**$_{[0.1\text{-}30\ ;\ 0.1\text{-}40m]}$) have higher average fluxes than the base case for their entire simulation runs. For **VPD**$_{[0.1\text{-}30m]}$, which ran for 3000 years and was producing flux after around 2000 years, the average flux is higher in the first half of that time, reaching ~1.6 mol/m^2/year but decreases in the second half (between 2500 and 3000 years) to ~0.8 mol/m^2/year. This suggests that the system had not yet reached steady state, with the increase in flux being the long term buildup of gas being released. Interestingly, **VPD**$_{[0.1\text{-}40m]}$ ran for 5000 years and was producing flux after ~3000 years, following the opposite pattern. The simulated case has an average of ~0.9 mol/m^2/year for the first 1000 years and ~1.6 mol/m^2/year for the final 1000 years. This latter increase in average flux may be the long term buildup of gas in the deepest parts of the sediments being released, suggesting **VPD**$_{[0.1\text{-}40m]}$ never reached steady state. The base case behaves more like **VPD**$_{[0.1\text{-}40m]}$, having a lower average in the first half of the flux period, this average then increasing in the second half. The average CH_4 for the base case is the same in the entire second half of the flux period for multiple different time windows, however, this was not the case for **VPD**$_{[0.1\text{-}30m]}$ nor **VPD**$_{[0.1\text{-}40m]}$. This makes it difficult to argue that either of the deep **VPD** simulations reached steady state during the simulated times. The average fluxes for different time windows for the **VPD** simulations are listed in Table 6.

Table 6. Average CH4 gas flux rates at different time points for VPD simulations

Average CH_4 gas flux (mol/m^2/year)	**VPD (base)** $_{[0.1\text{-}12.5m]}$	**VPD** $_{[0.1\text{-}30m]}$	**VPD** $_{[0.1\text{-}40m]}$
Entire flux period	0.93	1.28	1.31
First half of flux period	0.88	1.62	0.97
Second half of flux period	0.98	0.82	1.67
Steady state	0.98	-	-

For the vertical resolution tests, the model seems to converge at around 960 grid cells (**R**$_{2.64\ cm}$). The lower resolutions had stronger bands at lower frequencies, as seen in Figure 12. These low resolutions had fewer fractures (Figure 13), which is what probably caused this effect. For the base case and above, although there is a slightly lower saturation for the PFZ in the higher resolution cases, the spread of fractures and the frequency distribution is quite similar. From this we suggest that the model converges at the very least between 960 and 1080 grid cells (**R**$_{[2.45\ ;\ 2.35\ cm]}$).

5.2 Previous studies

Previous studies have researched different aspects of the dynamics of the methane production and flux at the Landsort deep. In situ sampling has given estimates toward CH_4 production (modeled using porewater samples), geochemical surveys for measuring diffusive fluxes and AOM dynamics such as the SMTZ depth (Egger et al., 2017; Ketzer et al., 2024). Acoustic data has been interpreted to infer CH_4 gas flux and free gas depth (Christian Stranne, personal communication, 2026; Figure 2).

The modeled CH_4 production by Egger et al., (2017) is at least five times lower than our base case and has two distinct peaks, at ~6 and ~20m. The **VPD** for our base case was based on the depth of the first peak, but the deeper peak, as shown in the results for case $\mathbf{VPD}_{[0.1\text{-}40m]}$, introduces bursts of methane that are exceptionally high (up to >100 mol / m^2 / year), which is 100 to 10 times higher than the suggested average (1 - 10 mol / m^2 / year from acoustic surveys). This suggests that although a deeper methane production may exist, it is unlikely to contribute to seepage.

Diffusive fluxes measured by Ketzer et al., (2024) to ~6.06 mol / m^2 / year are certainly interesting for things such as AOM or diffusive flux modelling, it is different from CH_4 gas flux which is what is modeled in this study. The SMTZ was also measured in that study to be < 20 and up to <10 cm in this area. From acoustic data the free gas depth can be interpreted approximately to range between ~9m to ~5m at the seep site.

More broad studies focusing on baltic sea methane dynamics include geochemical investigations and acoustic surveys, such as sampling sediments for chemical signals used to determine the SMTZ and methane dynamics along an acoustic transect measuring the free gas depths in the southern Baltic sea (Flury et al., 2016; Dale et al., 2019; Lapham et al., 2024). These studies report similar findings, mainly the inhibition and or bypass of the AOM filter due to fractures and geochemistry and the depth of the SMTZ and its coupling to the rate of organic matter breakdown. These are factors that were not modeled in this paper, but they provide context to the general methane - AOM dynamics in the baltic sea, which is why they are discussed here.

Previous work has been done in TOUGH+HYDRATE regarding fracture dynamics as well as AOM inhibition with temperature forcing on gas hydrate systems (Stranne et al., 2017; Stranne et al., 2022;), which is still relevant to this work since they can be used to predict behaviours the system when tuning different parameters.

We were able to see very sensitive behaviour in our modelling that was not reported in previous studies, presumably since we used a comparatively light source of CH_4 over a much longer time scale. Regarding the fracture module, changes in $\boldsymbol{k_f}$ affect the time of first gas release somewhat. $\boldsymbol{k_f}_{[10^{-11} m^2]}$ takes the longest time to start the gas release, with time decreasing with increasing $\boldsymbol{k_f}$. . Changes in $\boldsymbol{\lambda}^*$ did have an effect on flux, something that Stranne et al., (2017) does not report. Since the position of the source and the PFZ so delicately affect the flux when in the mixed flow regime, small changes of the PFZ in this study changes the flux dramatically.

This study, by coupling things such as fracture dynamics with the methanogenesis and other geochemical observations, contributes new approaches in understanding the dynamics of this and similar systems.

5.3 Model limitations

As stated in section 2.4, the model is in 1 dimension, which for fracture propagation becomes a bit esoteric. In real life, gas plumes rarely come from the same spot for long amounts of time, and fractures are known to also propagate horizontally (not seldom through existing weaknesses in the sediments such as fault planes or slip surfaces (Liu et al., 2022)), something that a 1D simulation cannot account for. To visualize it, one can imagine the model as simulating the entire seepage area's average behaviour over time, or as being positionally independent and just showing the state of the actively seeping parts when said seepages are occurring. Then it is a bit clearer what fractures in the model actually represent, as their horizontal location does not matter.

The model's physical properties are also implemented as one value for the whole column. Things such as permeability, grain density and porosity are assumed to be the same for 400 meters. While we are only modelling no more than 12.5m most of the cases in this study, this is still a simplification.

The implemented methanogenesis model is also a simplification of real life methanogenesis. In the area, multiple factors in the sediments control methane production and its depths, such as metals contents (Egger et al., 2017), depth of the SMTZ , bottom water oxygen content and sedimentation rate (Ketzer et al., 2024) which means that the production is not a constant rate in real life.

5.4 Implications and future work

Observations have been made of increased gas bubbling after sea level reduction in the area, with a time lag of a couple of days. This might be, if the PFZ theory is correct, due to a reduction in the pressure from above reducing the vertical stress and thus lowering the PFZ, leading to a faster seepage of methane. Future modelling could introduce a sea level reduction after observations to test this. Further modelling of CH_4 production in these sediments in order to find the correct depth profile would help to understand the dynamics of this system, as well as a focused study on the flow regimes.

Long time series with ebullition data do not exist at this time. Thus in situ observations of gas bubbles for a prolonged time are needed in order to investigate some results from this modelling. A physical survey of the moat, on the east hand side of the seep site can be conducted in order to understand the dynamics of the permanently fractured zone. By using the argued for here relationship between porosity and the PFZ, future research could determine physical properties using acoustic midwater data on sediments containing gas by measuring the free gas depth.

6. Conclusions

When starting the modelling project, the research goal was initially to model the observed CH_4 flux at the landsort deep seep site to see if such modelling is possible in TOUGH+HYDRATE. As the project grew, some other things also became important as they revealed themselves, such as the sensitive relationship between the PFZ depth and the depth of the methanogenesis, and finding how sensitive the PFZ depth was to other previously untested parameters such as the grain density and porosity. Other things were shown to not be as significant as was initially thought, such as being able to analyze high frequency fluxes on a timescale of days and / or weeks. From the findings presented we draw five conclusions in no particular order of importance:

1: Modelling observed methane fluxes at the Landsort deep seep site is possible in TOUGH+HYDRATE. The results indicate a production at least 5 times higher than in the nearby study area of Egger et al., (2017).

2: The largest control of the onset of gas release and average flux rate is the rate of CH_4 production in the methanogenesis module, followed shortly by the **VPD**.

3: The flow regime is primarily controlled by the vertical CH_4 production distribution and depth of the PFZ. More exactly, the relative position of the CH_4 production to the PFZ. If the production takes place more or less entirely inside the PFZ the flow regime is a constant seepage after reaching steady state, as in cases where $\boldsymbol{\lambda}^* \leq 1$. If a larger part of the production exists underneath the PFZ, the flow regime switches to a build up- burst regime, controlled by fracture release and overpressure. The deeper the source is, the larger and less common the bursts are.

4: The frequency of flux is primarily determined by the flow regime, rather than by individual parameters. While some observed changes in periodicity for the flux are introduced by accelerating gas migration and accumulation when tuning parameters such as the fracture permeability and the methane production source, these do not fundamentally determine the character of the seepage. Instead, the previously mentioned flow regimes, controlled by the position of the PFZ relative to the **VPD**, are the dominant controls on the periodicity. Continuous seepages will lead to non periodic fluxes, while fracture flow introduces periodicity. The significance of the observed frequency of fluxes are not known, since the research goal ultimately was to find frequencies in fluxes over days and weeks, and the results show much longer periods, thus more data with longer time series is needed to investigate the validity of these findings.

5: The depth of the PFZ is very sensitive to small changes in sediment porosity, sediment cohesion and tensile strength, the latter two in the model are represented by the fracture threshold ($\boldsymbol{\lambda}^*$). The spatial variability in PFZ depths can be reasonably explained by changes in $\boldsymbol{\Phi}$, $\boldsymbol{\lambda}^*$ and $\boldsymbol{\varrho}$, while the slight variation in in seafloor depth has negligible effect.

We hope that this shows that modelling methane fluxes in the landsorts deep and other similar non-hydrate methane seepage spots is not only possible, but actually helpful to understand the dynamics of seepage systems. One could, for example, assume certain physical properties of sediments such as porosity or grain density by finding the free gas depth in acoustic data, should this actually be as sensitive in real life as it is in the model.

7. Acknowledgements

I want to thank my supervisor, Associate Professor Christian Stranne, for guiding me through this modelling endeavor, and for trusting me with exploring new ideas. Although it has been a challenge at times to grasp every concept, Challenges are a great motivator!

I also want to thank Professor Matt O'Reagan for being very helpful with the calculations of the physical properties, as well as providing the data for EL26-LD2-6GC3 gravity core, as well as Associate professor Richard Gyllencreutz for taking the time to help me with the frequency analysis, and Professor Helen Coxall for discussing the art of writing scientific articles

Special thanks also to Vicent Doñate, PhD, for being helpful and providing the bathymetric data and the overview map.

Lastly, Thank you to Björn Eriksson, head of IGV's IT department, for providing me with the necessary infrastructure to perform my work. This could not have been made without them.

8. References
8.1 Literature

Barker Jørgensen, B., Egger, M., & Canfield, D. E. (2024). Sulfate distribution and sulfate reduction in global marine sediments. *Geochimica et Cosmochimica Acta*, *364*, 79–88. https://doi.org/10.1016/j.gca.2023.11.015

Behrmann, J. H., Flemings, P. B., John, C. M., & the IODP Expedition 308 Scientists. (2006). Rapid Sedimentation, Overpressure, and Focused Fluid Flow, Gulf of Mexico Continental Margin. *Scientific Drilling*, *3*, 12–17. https://doi.org/10.5194/sd-3-12-2006

Boudreau, B. P. (2012). The physics of bubbles in surficial, soft, cohesive sediments. *Marine and Petroleum Geology*, *38*(1), 1–18. https://doi.org/10.1016/j.marpetgeo.2012.07.002

Bullard, E. C. (1939). Heat flow in South Africa. *Proceedings of the Royal Society of London. A. Mathematical and Physical Sciences*, *173*(955), 474–502. https://doi.org/10.1098/rspa.1939.0159

Daigle, H., Cook, A., Fang, Y., Bihani, A., Song, W., & Flemings, P. B. (2020). Gas-Driven Tensile Fracturing in Shallow Marine Sediments. *Journal of Geophysical Research: Solid Earth*, *125*(12), e2020JB020835. https://doi.org/10.1029/2020JB020835

Daigle, H., & Dugan, B. (2011). Capillary controls on methane hydrate distribution and fracturing in advective systems. *Geochemistry, Geophysics, Geosystems*, *12*(1). https://doi.org/10.1029/2010GC003392

Dale, A. W., Flury, S., Fossing, H., Regnier, P., Røy, H., Scholze, C., & Jørgensen, B. B. (2019). Kinetics of organic carbon mineralization and methane formation in marine sediments (Aarhus Bay, Denmark). *Geochimica et Cosmochimica Acta*, *252*, 159–178. https://doi.org/10.1016/j.gca.2019.02.033

Doñate Felip, V., Ketzer, M., Ladroit, Y., Jakobsson, M., O'Regan, M., Humborg, C., and Stranne, C.: One of Europe's largest methane ebullition field lies at 400 m below sea level in the Baltic Sea., EGU General Assembly 2025, Vienna, Austria, 27 Apr–2 May 2025, EGU25-19885, https://doi.org/10.5194/egusphere-egu25-19885, 2025.

Egger, M., Hagens, M., Sapart, C. J., Dijkstra, N., van Helmond, N. A. G. M., Mogollón, J. M., Risgaard-Petersen, N., van der Veen, C., Kasten, S., Riedinger, N., Böttcher, M. E., Röckmann, T., Jørgensen, B. B., & Slomp, C. P. (2017). Iron oxide reduction in methane-rich deep Baltic Sea sediments. *Geochimica et Cosmochimica Acta*, *207*, 256–276. https://doi.org/10.1016/j.gca.2017.03.019

Flury, S., Røy, H., Dale, A. W., Fossing, H., Tóth, Z., Spiess, V., Jensen, J. B., & Jørgensen, B. B. (2016). Controls on subsurface methane fluxes and shallow gas formation in Baltic Sea sediment (Aarhus Bay, Denmark). *Geochimica et Cosmochimica Acta*, *188*, 297–309. https://doi.org/10.1016/j.gca.2016.05.037

Howarth, R. W., Santoro, R., & Ingraffea, A. (2011). Methane and the greenhouse-gas footprint of natural gas from shale formations. *Climatic Change*, *106*(4), 679–690. https://doi.org/10.1007/s10584-011-0061-5

Howarth, R. W. (2014). A bridge to nowhere: Methane emissions and the greenhouse gas footprint of natural gas. *Energy Science & Engineering*, *2*(2), 47–60. https://doi.org/10.1002/ese3.35

Judd, A. G. (2004). Natural seabed gas seeps as sources of atmospheric methane. *Environmental Geology*, *46*(8), 988–996. https://doi.org/10.1007/s00254-004-1083-3

Ketzer, M., Stranne, C., Rahmati-Abkenar, M., Shahabi-Ghahfarokhi, S., Jaeger, L., Pivel, M. A. G., Josefsson, S., & Zillén, L. (2024). Near seafloor methane flux in the world's largest human-induced dead zone is regulated by sediment accumulation rate. *Marine Geology*, *468*, 107220. https://doi.org/10.1016/j.margeo.2024.107220

Knittel, K., & Boetius, A. (2009). Anaerobic oxidation of methane: Progress with an unknown process. *Annual Review of Microbiology*, *63*, 311–334. https://doi.org/10.1146/annurev.micro.61.080706.093130

Koh, C. A., Westacott, R. E., Zhang, W., Hirachand, K., Creek, J. L., & Soper, A. K. (2002). Mechanisms of gas hydrate formation and inhibition. *Fluid Phase Equilibria, Proceedings of the Ninth International Conference on Properties and Phase Equilibria for Product and Process Design*, *194–197*, 143–151. https://doi.org/10.1016/S0378-3812(01)00660-4

Lapham, L. L., Lloyd, K. G., Fossing, H., Flury, S., Jensen, J. B., Alperin, M. J., Rehder, G., Holzhueter, W., Ferdelman, T., & Jørgensen, B. B. (2024). Methane leakage through the sulfate–methane transition zone of the Baltic seabed. *Nature Geoscience*, *17*(12), 1277–1283. https://doi.org/10.1038/s41561-024-01594-z

Lenstra, W. K., van Helmond, N. A. G. M., Martins, P. D., Wallenius, A. J., Jetten, M. S. M., & Slomp, C. P. (2023). Gene-Based Modeling of Methane Oxidation in Coastal Sediments: Constraints on the Efficiency of the Microbial Methane Filter. *Environmental Science & Technology*, *57*(34), 12722–12731. https://doi.org/10.1021/acs.est.3c02023

Lipka, M., Woelfel, J., Gogina, M., Kallmeyer, J., Liu, B., Morys, C., Forster, S., & Böttcher, M. E. (2018). Solute Reservoirs Reflect Variability of Early Diagenetic Processes in Temperate Brackish Surface Sediments. *Frontiers in Marine Science*, *5*. https://doi.org/10.3389/fmars.2018.00413

Liu, H., Zhan, L., & Lu, H. (2022). Mechanisms for upward migration of methane in marine sediments. *Frontiers in Marine Science*, *9*. https://doi.org/10.3389/fmars.2022.1031096

Lomb, N. R. (1976). Least-squares frequency analysis of unequally spaced data. *Astrophysics and Space Science*, *39*(2), 447–462. https://doi.org/10.1007/BF00648343

Moridis, G. J. (2014). *User's manual for the hydrate v1. 5 option of TOUGH+ v1. 5: A code for the simulation of system behavior in hydrate-bearing geologic media*. (LBNL--6869E, 1165986; p. LBNL--6869E, 1165986). https://doi.org/10.2172/1165986

Pardo-Igúzquiza, E., & Rodríguez-Tovar, F. J. (2013). Spectral analysis of uneven time series of geological variables. *Boletín Geológico y Minero*, *124*(2), 323–337. https://doi.org/10.21701/bolgeomin.124.2.011

Reeburgh, W. S. (2007). Oceanic Methane Biogeochemistry. *Chemical Reviews*, *107*(2), 486–513. https://doi.org/10.1021/cr050362v

Riedinger, N., Formolo, M. J., Lyons, T. W., Henkel, S., Beck, A., & Kasten, S. (2014). An inorganic geochemical argument for coupled anaerobic oxidation of methane and iron reduction in marine sediments. *Geobiology*, *12*(2), 172–181. https://doi.org/10.1111/gbi.12077

Ruppel, C. D., & Kessler, J. D. (2017). The interaction of climate change and methane hydrates. *Reviews of Geophysics*, *55*(1), 126–168. https://doi.org/10.1002/2016RG000534

Rönnberg, C., & Bonsdorff, E. (2004). Baltic Sea eutrophication: Area-specific ecological consequences. *Hydrobiologia*, *514*(1), 227–241. https://doi.org/10.1023/B:HYDR.0000019238.84989.7f

Scargle, J. D. (1982). Studies in astronomical time series analysis. II. Statistical aspects of spectral analysis of unevenly spaced data. In *The Astrophysical Journal* (Vol. 263, pp. 835–853). IOP.

Stranne, C., O'Regan, M., Hong, W.-L., Brüchert, V., Ketzer, M., Thornton, B. F., & Jakobsson, M. (2022). Anaerobic oxidation has a minor effect on mitigating seafloor methane emissions from gas hydrate dissociation. *Communications Earth & Environment*, *3*(1), 163. https://doi.org/10.1038/s43247-022-00490-x

Stranne, C., O'Regan, M., & Jakobsson, M. (2017). Modeling fracture propagation and seafloor gas release during seafloor warming-induced hydrate dissociation. *Geophysical Research Letters*, *44*(16), 8510–8519. https://doi.org/10.1002/2017GL074349

VanderPlas, J. T. (2018). Understanding the Lomb–Scargle Periodogram. *The Astrophysical Journal Supplement Series*, *236*(1), 16. https://doi.org/10.3847/1538-4365/aab766

Weber, T., Wiseman, N. A., & Kock, A. (2019). Global ocean methane emissions dominated by shallow coastal waters. *Nature Communications*, *10*(1), 4584. https://doi.org/10.1038/s41467-019-12541-7

Winterhalter, B., Flodén, T., Ignatius, H., Axberg, S., & Niemistö, L. (1981). Chapter 1 Geology of the Baltic Sea. In A. Voipio (Ed.), *Elsevier Oceanography Series* (Vol. 30, pp. 1–121). Elsevier. https://doi.org/10.1016/S0422-9894(08)70138-7

8.2 Data sources

EMODnet Bathymetry Consortium (2024).EMODnet Digital Bathymetry (DTM 2024). https://doi.org/10.12770/cf51df64-56f9-4a99-b1aa-36b8d7b743a1

Expedition 347 Scientists. (2014). *Core summary for IODP Hole 347-M0063A* [Dataset]. PANGAEA. https://doi.org/10.1594/PANGAEA.837787

Expedition 347 Scientists. (2014). *Core summary for IODP Hole 347-M0063B* [Dataset]. PANGAEA. https://doi.org/10.1594/PANGAEA.837788

Expedition 347 Scientists. (2014). *Core summary for IODP Hole 347-M0063C* [Dataset]. PANGAEA. https://doi.org/10.1594/PANGAEA.837789

Expedition 347 Scientists. (2014). *Core summary for IODP Hole 347-M0063D* [Dataset]. PANGAEA. https://doi.org/10.1594/PANGAEA.837790

Expedition 347 Scientists. (2014). *Core summary for IODP Hole 347-M0063E* [Dataset]. PANGAEA. https://doi.org/10.1594/PANGAEA.837791

Expedition 347 Scientists. (2014). *Physical properties of IODP Hole 347-M0063A* [Dataset]. PANGAEA. https://doi.org/10.1594/PANGAEA.838477

Expedition 347 Scientists. (2014). *Physical properties of IODP Hole 347-M0063B* [Dataset]. PANGAEA. https://doi.org/10.1594/PANGAEA.838478

Expedition 347 Scientists. (2014). *Physical properties of IODP Hole 347-M0063C* [Dataset]. PANGAEA. https://doi.org/10.1594/PANGAEA.838479

Expedition 347 Scientists. (2014). *Physical properties of IODP Hole 347-M0063D* [Dataset]. PANGAEA. https://doi.org/10.1594/PANGAEA.838480

Expedition 347 Scientists. (2014). *Physical properties of IODP Hole 347-M0063E* [Dataset]. PANGAEA. https://doi.org/10.1594/PANGAEA.838481

Expedition 347 Scientists. (2014). *Thermal conductivity of IODP Hole 347-M0063A* [Dataset]. PANGAEA. https://doi.org/10.1594/PANGAEA.838821

Expedition 347 Scientists. (2014). *Thermal conductivity of IODP Hole 347-M0063D* [Dataset]. PANGAEA. https://doi.org/10.1594/PANGAEA.838822

Expedition 347 Scientists. (2014). *Moisture and density (MAD) measured on IODP Hole 347-M0063A* [Dataset]. PANGAEA. https://doi.org/10.1594/PANGAEA.838358

Expedition 347 Scientists. (2014). *Moisture and density (MAD) measured on IODP Hole 347-M0063B* [Dataset]. PANGAEA. https://doi.org/10.1594/PANGAEA.838359

Expedition 347 Scientists. (2014). *Moisture and density (MAD) measured on IODP Hole 347-M0063C* [Dataset]. PANGAEA. https://doi.org/10.1594/PANGAEA.838360

Expedition 347 Scientists. (2014). *Moisture and density (MAD) measured on IODP Hole 347-M0063D* [Dataset]. PANGAEA. https://doi.org/10.1594/PANGAEA.838361

Expedition 347 Scientists. (2014). *Moisture and density (MAD) measured on IODP Hole 347-M0063E* [Dataset]. PANGAEA. https://doi.org/10.1594/PANGAEA.838362